Geochemistry 80 (2020) 125630

Contents lists available at ScienceDirect

Geochemistry

journal homepage: www.elsevier.com/locate/chemer

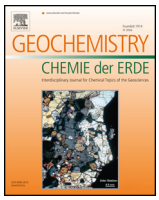

Temporal changes in geochemical-isotopic systematics of the late Pleistocene Akkaya travertines (Turkey) – Implications for fluid flow circulation and seismicity

Gokhan Yıldırım[a], Halim Mutlu[a,*], Volkan Karabacak[b], I. Tonguç Uysal[a], Kadir Dirik[c], Abidin Temel[c], Galip Yüce[c], Jian-xin Zhao[d]

[a] Ankara University, Geological Engineering Department, Gölbaşı, Ankara, Turkey
[b] Eskişehir Osmangazi University, Geological Engineering Department, Eskişehir, Turkey
[c] Hacettepe University, Geological Engineering Department, Beytepe, Ankara, Turkey
[d] Radiogenic Isotope Facility, School of Earth and Environmental Sciences, University of Queensland, Brisbane, Australia

ARTICLE INFO

Handling Editor: Martin Dietzel

Keywords:
U-Th dating
Stable isotope
Geochemistry
Helium
Akkaya travertine
North Anatolian Fault Zone
Turkey

ABSTRACT

We investigate the temporal variations in stable carbon and oxygen and radiogenic Sr isotope as well as rare earth element contents of Akkaya travertine deposits in the Eskipazar region, northwest Turkey. U-Th age data indicate that studied travertines in the periphery of the 1944-earthquake rupture of the North Anatolian Fault Zone formed in a time span of 93 to 1.8 ka BP. The younger group is represented by fissure-filling carbonates whereas the older sequence is composed of veins with varying crystallization ages that are injected to bedded travertines. The age data on vein injections and fissure-ridge travertines in the Akkaya site indicate the seismic reactivation along the west-central part of the North Anatolian Fault Zone to be intensified at least 4 periods (1.8, 20, 47 and 88 ka BP) during the last 90 ka.

$\delta^{18}O$ and $\delta^{13}C$ systematics of Akkaya travertines, which are precipitated by CO_2–rich fluids depressurized during episodic seismic unrest, are in the range from −15.86 to −7.67‰ (VPDB) and 4.66–8.68‰ (VPDB), respectively. $\delta^{18}O$ of the fluid equilibrating with the studied travertines is estimated in the range of −11.2 to −10.2‰ which is quite consistent with the average value (−12.3‰) reported for the Akkaya thermal spring. Stable isotope values of travertines indicate modification by rapid CO_2 degassing associated with seismic events. Helium isotope compositions of gas phase and dissolved gas of thermal fluids in the area refer to mantle contribution up to 12 %. Sr isotope values of Akkaya travertines are probably originated from Upper Cretaceous marine limestones or mafic basement rocks. REY contents are about 3 orders of magnitude lower than those of basement lithologies.

1. Introduction

Turkey is located in one of the most tectonically active regions in the world (Şengör and Yilmaz, 1981; Bozkurt, 2001). This is manifested by mantle degassing (Güleç et al., 2002) associated with a long-lasting seismic activity and a large number of hot springs emerging along the major active fault zones throughout Anatolia (Mutlu and Güleç, 1998). Travertine deposits are very common in regions of tectonic unrest where a variety of fault systems transfer the CO_2-rich fluids to the surface (Sibson et al., 1975; Hancock et al., 1999; D'Alessandro et al., 2007). These fluids with pressurized CO_2 form a complex network of carbonate veins and even breccia deposits within travertine bodies (Robert et al., 1995; Cox, 2007; Uysal et al., 2009). Travertine is a very informative deposit since it allows determining not only the timing of crystallization but also the source and temperature of calcite-precipitating fluid. Oxygen isotope fractionation between carbonate and water (e.g., Friedman and O'Neil, 1977; Coplen, 2007; Kele et al., 2011) and clumped isotope thermometer methods (e.g., Kele et al., 2015; Kluge et al., 2018) are widely used for the estimation of paleotemperatures from a range of carbonate minerals. Despite a large number of studies, there are still challenges in obtaining reliable temperature data from the application of isotope fractionation and Δ47 techniques (Kele et al., 2015; Jones and Peng, 2016).

The collision between the Eurasian and the Arabian plates gave rise to westward tectonic escape of Anatolia along two major transform faults, the right-lateral North Anatolian Fault Zone (NAFZ) and the left-

* Corresponding author.
E-mail address: halimmutlu@ankara.edu.tr (H. Mutlu).

https://doi.org/10.1016/j.chemer.2020.125630
Received 29 September 2019; Received in revised form 4 March 2020; Accepted 16 March 2020
Available online 30 April 2020

lateral East Anatolian Fault Zone (Mc Kenzie, 1972). Accordingly, Anatolia, where the compressional regime is transformed to extensional tectonics towards the west, is one of the most rapidly deforming regions in the world. As a part of the Alpine-Himalayan orogenic belt, Turkey hosts vast number of geothermal fields in areas of seismic unrest where fossil and modern travertines have been deposited. Previous studies demonstrated that several travertine sites along the major fault zones in Anatolia contain fissure-filling carbonates and breccia fills. These deposits were formed during the last 500,000 years (Late Quaternary) from fluids of high-CO_2 content (Hancock et al., 1999; Uysal et al., 2007, 2009, 2011; Ünal-İmer et al., 2016; Karabacak et al., 2017). Natural CO_2 accumulation is vitally important for investigation of geological factors that control emission and evolution of CO_2 in the crust (Pearce et al., 2006; Ünal–İmer et al., 2016). Studies on the source of CO_2 in travertine sites have provided new insights into understanding of vein growth mechanism and shown that active tectonics exerts a major control on the CO_2 discharge (Uysal et al., 2007, 2009, 2011; Ünal–İmer et al., 2016; Karabacak et al., 2017). In this sense, U-series method has become a routine technique to date fissure-filling carbonate deposits and associated fluid flow in seismically active areas (e.g., Uysal et al., 2007; Nuriel et al., 2011; Ünal–İmer et al., 2016). The $^{87}Sr/^{86}Sr$ ratios, and stable isotope ($\delta^{13}C$-$\delta^{18}O$) compositions and rare earth element contents measured on travertines provide a better understanding of fluid flow that greatly control the vein precipitation.

Although the timing of fissure generation in vein systems in the western (e.g. Uysal et al., 2007, 2011; Özkul et al., 2013; Ünal–İmer et al., 2016) and central Anatolia (Uysal et al., 2009; Karabacak et al., 2017) have been well studied, limited data are available for the travertine sites along the NAFZ (Gökten et al., 2011). Therefore, the present study will greatly contribute to the geochemical characteristics and the origin of fluids that formed travertine deposits along the west-central part of the NAFZ which is one of the best-known and largest active continental fault systems in the world. In this study, we present the results of U-series ages of carbonate samples collected from the Akkaya travertine site in the Eskipazar region, northern Turkey (Fig. 1a,b). Ascertainment of seismic frequency of the NAFZ in this area is very important to understand the evolution of tectonic regime considering that limited data exist on the late Quaternary tectonic unrest along the NAFZ. Additionally, carbon, oxygen and Sr isotope compositions and REE chemistry of samples from the Akkaya travertine are discussed in regard to temporal variations in the source region and temperature of paleo-fluids. Moreover, helium isotope ($^3He/^4He$) compositions of thermal waters that recently precipitate the Akkaya travertines are used to investigate the noble gas contribution from various earth reservoirs (e.g. crust or mantle).

2. Material and method

We modified the previous structural maps in the vicinity of study area (i.e. Biryol, 2004; Karabacak et al., 2011; Emre et al., 2011) using digital elevation data at ca. 29-m ground pixel resolutions (AsterGDEM v2) (Fig. 1a). The key morphological lineaments were determined by satellite images (from Google Earth software) (Fig. 1b). The geological map was improved from Yücel and Hakyemez (1991), Şaroğlu et al. (1995) and Biryol (2004) on the basis of authors' field observations in the area shown in Fig. 2.

Fresh surfaces of detritus-free, crystalline vein travertines were sampled. Mineralogical compositions of travertine samples were resolved by both petrographic determinations and XRD (whole rock) analyses. Whole-rock XRD analyses were carried out at the Hacettepe University laboratories using a Rigaku D/MAX 2200 PC X-ray powder diffractometer with Ni-filtered CuK_α radiation at tube voltage and current of 40 kV and 40 mA, and a goniometer speed of 2°/min. Microscopic examinations on a total of 10 thin sections of carbonate samples were performed with James Swift (England) MP3500A polarizing microscope at the Geology Department of the Hacettepe University.

Fluid (gas and water phase) samples were collected from bubbling hot springs into glass containers and annealed copper tubes which were sealed in the field using a cold welding tool. The elemental and isotope compositions of samples were analyzed at the Istituto Nazionale di Geofisica e Vulcanologia (INGV), Sezione di Palermo, Italy. He-isotope ratio in samples was analyzed directly from the sample containers after purification in the high-vacuum inlet line of the mass spectrometer. The isotope composition of dissolved He was analyzed by headspace equilibration, following the method proposed by Inguaggiato and Rizzo (2004). He and Ne were then cryogenically separated and admitted into mass spectrometers. Briefly, neon (^{20}Ne) and helium (^3He and ^4He) isotopes were separated under a cryogenic trap that was initially cooled at ~8°K and then heated to ~41 and ~75°K to release helium and neon, respectively. The $^3He/^4He$ ratio and ^{20}Ne content were analyzed by a GVI Helix SFT mass spectrometer.

Travertine samples were dated by U-series technique at the Radiogenic Isotope Laboratory at the University of Queensland using a Nu Plasma HR Multicollector Inductively Coupled Plasma Mass Spectrometer (MCICP- MS) following the analytical protocols described in Zhao et al. (2001) and Ünal–İmer et al. (2016). $^{230}Th/^{238}U$ and $^{234}U/^{238}U$ ratios were computed using decay constants proposed by Cheng et al. (2000). U-series ages were estimated using the Isoplot/Ex 3.0 Program (Ludwig, 2003).

Sr isotopic compositions of samples were measured on the same MC-ICP-MS at the Radiogenic Isotope Laboratory of the University of Queensland. Sr isotope ratios were corrected for mass discrimination using the ratio of $^{86}Sr/^{88}Sr = 0.1194$. The repeated analyses of the SRM 987 international standard yielded a mean $^{87}Sr/^{88}Sr$ value of 0.710249 ± 0.00002 (2σ).

$\delta^{18}O$ and $\delta^{13}C$ values of carbonate samples were measured using an automated carbonate preparation device (KIEL-III) coupled to a gas-ratio mass spectrometer (Finnigan MAT 252) at the Environmental Isotope Laboratory of the University of Arizona (USA). Samples were reacted with dehydrated phosphoric acid (H_3PO_4) under vacuum at 70 °C. The isotope ratio measurement is calibrated based on repeated measurements of international standards NBS-19 and NBS-18 and analytical precision is ± 0.1‰ for $\delta^{18}O$ and ± 0.08‰ for $\delta^{13}C$ (1σ).

The trace element analyses of the carbonate samples were performed on a Thermo X-series ICP-MS (Radiogenic Isotope Laboratory, the University of Queensland) in high performance mode with instrument conditions as described in Lawrence and Kamber (2006), after dissolving the carbonates in a 2% HNO_3 solution embed with internal standards. The raw data were corrected for the low, detectable blank, internal and external drift, and for oxides and doubly charged species. Instrument response was calibrated against two independent digests of the USGS reference W-2, and confirmed by analysis of other inter-lab references, treated as unknowns. Corrections were applied for oxides using formation rates determined from pure single element REE standards.

3. Geological setting

The NAFZ represents ca.1200 km-long dextral strike-slip fault zone in land bordering the Eurasian Plate to the north and the Anatolian block to the south (Fig. 1a). It is composed of a series of right lateral strike-slip segments extending from eastern Anatolia to the northern Aegean Sea (McKenzie, 1972) (Fig. 1a). Because of its remarkable seismic activity and the importance for the Neotectonics of the eastern Mediterranean region, the NAFZ has been subjected to numerous geological, geomorphological and seismological studies.

The eastern sector of the NAFZ is limited to a narrow zone but widens to the west where shear is distributed to multiple parallel/subparallel segments (Şengör and Zabcı, 2019 and references therein) (Fig. 1a). For example, the 1944 earthquake along the Gerede segment of the NAFZ ruptured a number of parallel and subparallel fault

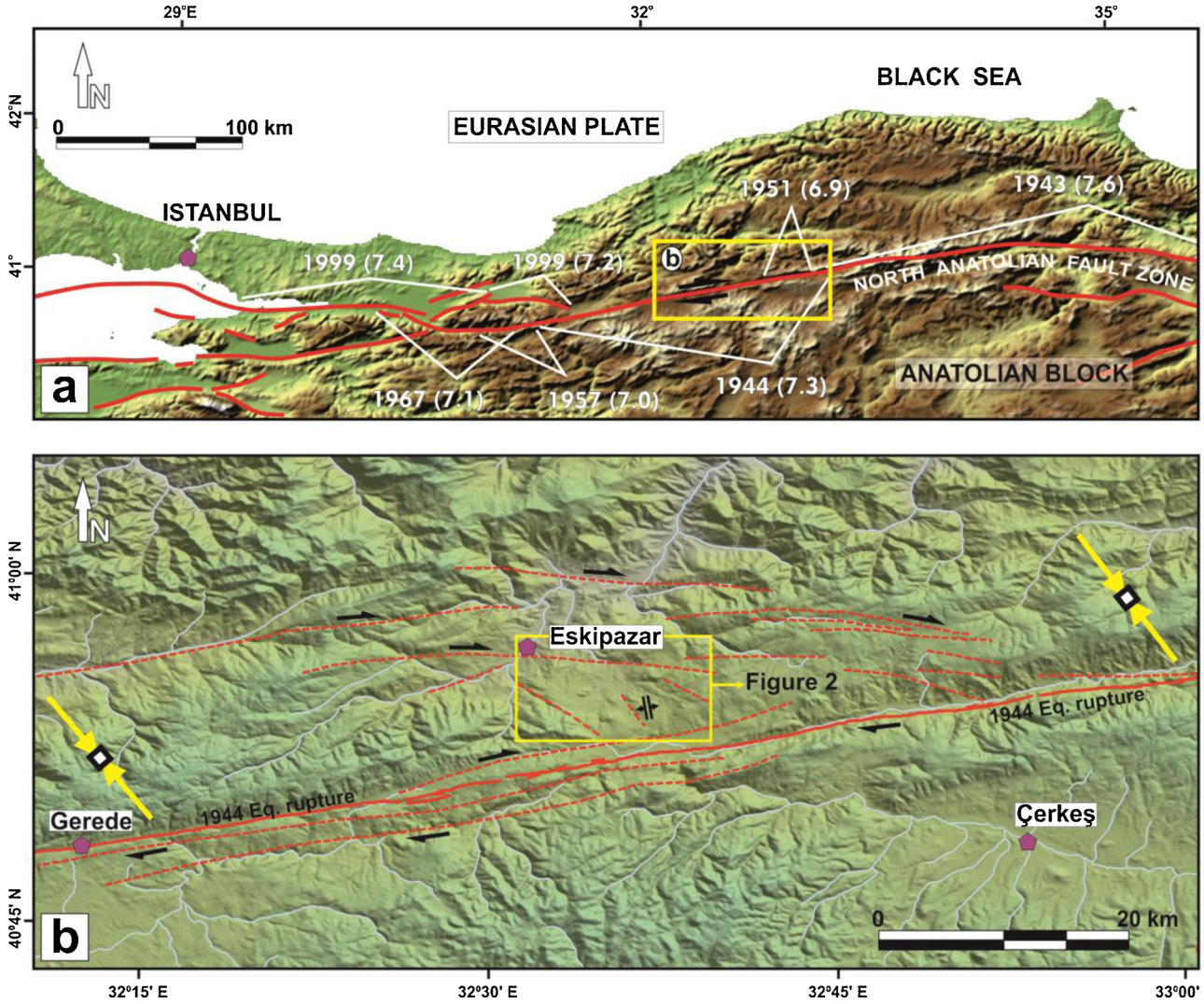

Fig. 1. (a) The west-central part of the North Anatolian Fault Zone showing recent major earthquakes (modified after Karabacak et al., 2011). (b) Shaded relief map of around the study area and general fault lineaments (it is generated using the SRTM digital data) Note that the dashed red lines show the faults (on the basis of authors' field observations) while solid line shows the 1944 Earthquake rupture (redrawn from Emre et al., 2011); blue lines show the streams; yellow arrows show the maximum horizontal compressional stress axis (S_{Hmax}) from the World Stress Map Project database (Heidbach et al., 2016).

segments of various lengths, ranging from 0.4 km to 22 km (Ayhan and Koçyiğit, 2010). Moreover, distributed deformation can take place over a wider zone than geologically specified. Regarding the 1944 Gerede earthquake, although geodetic data suggest that the width of the sheared deformation zone is 4.4 km, geologic observations reveal a much more limited width of 1 km (Kaduri et al., 2019).

The surface rupture of the 1944 Gerede earthquake is about 190-km-long (Fig. 1a) and it extends nearly 25 km along the valley of Gerede Stream between 32 °E and 33 °E (Fig. 1b). This strand striking ca. 80° extends westward to Bolu. Two parallel faults lie on the southern block and multiple parallel/subparallel branches are separated to the north at the 33 °E. The northern block is defined by E–W-striking right-lateral faults with numerous NW–SE-striking smaller faults representing extensional features in ca. 10–15 km-wide zone (Fig. 1). Typical fault-induced geomorphological features in the zone include dextrally deflected stream channel patterns and lineaments on the landscape (Fig. 1).

The study area is located nearly 6 km north of the 1944 earthquake rupture of the NAFZ (Fig. 1). Recent catastrophic seismic events with epicenters close to the Akkaya travertine such as 1944 Gerede (Mw = 7.6), the 1951 Kurşunlu (Mw = 7.2) earthquakes activated the NAFZ. Therefore, formation of Akkaya travertine is linked to reactivation of NAFZ in the late Quaternary (Biryol, 2004; Kuterdem, 2005).

The northern block of the 1944-earthquake segment consists of Late Cretaceous to Early Pliocene and Plio-Quaternary units. The Arkot Dağ Complex of Late Cretaceous age is the oldest rock unit in the study area (Fig. 2). It is an ophiolitic mélange consisting of several types of sedimentary, magmatic and metamorphic rocks which are well exposed along the Intra-Pontide suture zone (Tokay, 1973; Göncüoğlu et al., 2014). The complex widely covering a large area around Akkaya contains several limestone blocks of varying size.

The Galatian volcanites cropping out in a limited area at the eastern part of studied travertines (Fig. 2) is a part of volcanic belt extending at the northwest of central Anatolia. The evolution of these volcanics has been linked to the closure of the northern branch of the Neotethyan Ocean (Şengör and Yilmaz, 1981). They are represented by basalt and andesite lavas, pyroclastics and tuff layers of early to late Miocene age (Wilson et al., 1997).

The Galatian volcanites are unconformably overlain by the Eskipazar formation which starts with light-gray, thickly bedded lacustrine limestone continuing upward with the alternation of polygenetic, poorly lithified, poorly sorted conglomerates interbedded with thinly laminated red mudstones and sandy–pebbly mudstone horizons.

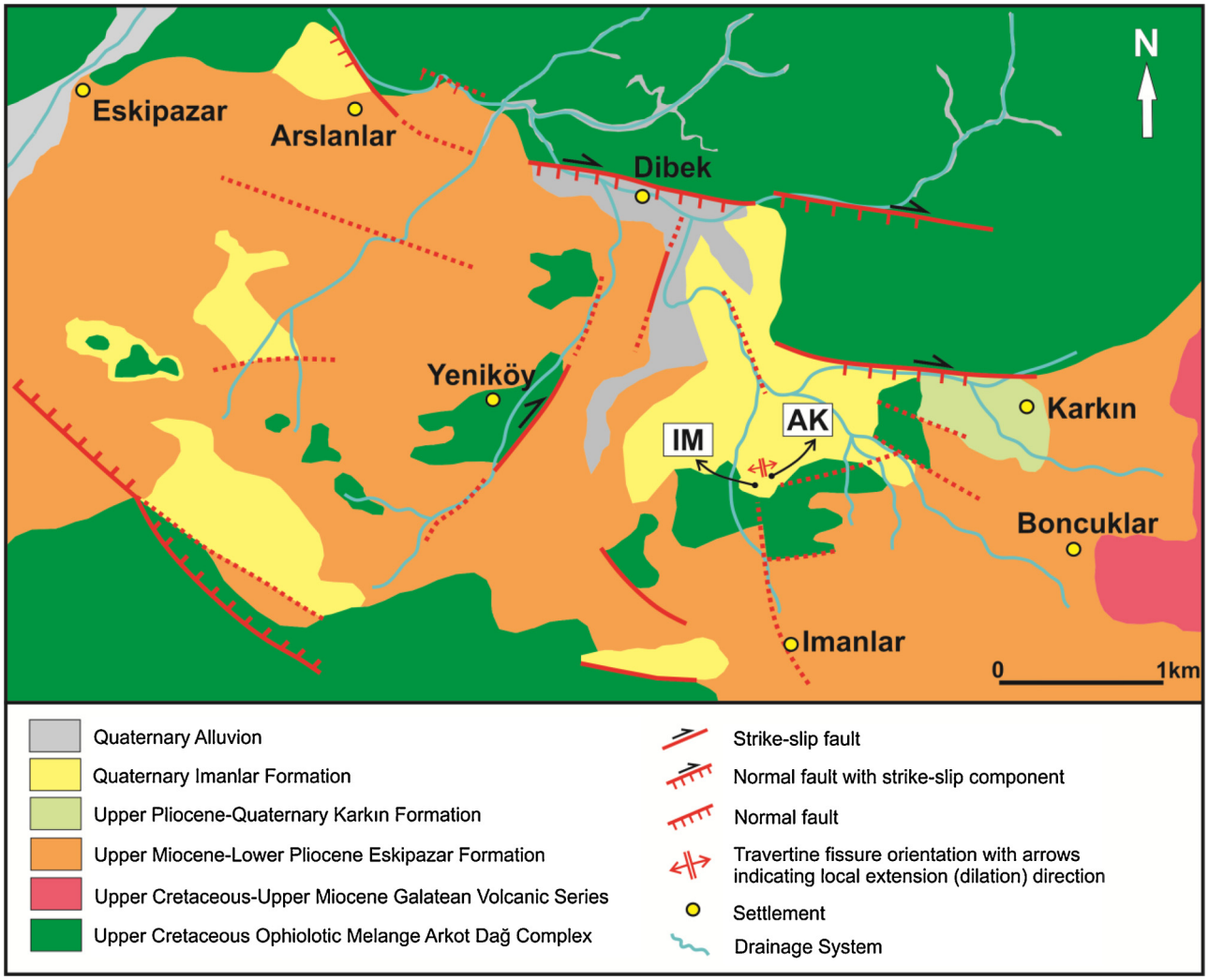

Fig. 2. Geological map of study area (modified from Yücel and Hakyemez (1991), Şaroğlu et al. (1995) and Biryol (2004) on the basis of authors' field observations). AK: Akkaya fissure-ridge travertine and IM: Imanlar bedded travertine (vein injections).

The pebbles consist chiefly of andesite, dunite, basalt, rhyolite, pelagic limestone, and radiolarites bounded by a silty matrix. Formation with thickness of about 500 m was deposited in a fluvio-lacustrine environment (Şaroğlu et al., 1995; Biryol, 2004). Micro and mammalian fossil assemblage in this formation yield late Miocene-early Pliocene age.

The Eskipazar formation is overlain by the Imanlar formation of Quaternary age which is represented by whitish-gray to yellowish, thickly-bedded lacustrine carbonates of Pliocene-Quaternary age. Calcite cement fills the highly porous parts of the unit. They laterally pass into loose, unsorted, well-rounded polygenetic terrace conglomerates composing of pelagic limestone and volcanic rock fragments set in a coarse-grained cement matrix. Recently precipitating fissure-ridge travertines are the youngest unit in the area (Fig. 2).

4. Results

4.1. Field characteristics of Akkaya travertines

The fissure-ridge travertine is very characteristic with its rather steep morphology. The ridge with a length of 90 m extends on a nearly NS-trending axis (Fig. 3a). The strike of ridge axis extends from N10W at the southern edge to N6W at the northern rim. The width of ridge ranges from 11 m at the south to 25 m to the north. Carbonate veins with thickness of 2–3 cm occur parallel to the fracture walls of older deposited travertines.

There are 3 bubbling hot springs manifested from pools of 1–2 m across at the northern edge of Akkaya fissure-ridge travertine (Fig. 3b). Following the 1944 Gerede earthquake, the locations of springs were shifted and the discharge rates decreased (Yücel and Hakyemez, 1991). The southern part of the ridge is dirty white-yellow colored whilst the northern part is much whiter due to ongoing travertine precipitation. Massive cascades are formed on both sides of travertine mound (e.g. Pentecost, 2005) and thickness of crystalline crusts (layers) on cascades is up to 20 cm (Fig. 3c).

The underlying bedded travertines (so called Imanlar travertine) are gray to white colored and made up of very thin horizontal carbonate layers (a few cm thickness) that are accompanied by clastic material and/or breccias. The Imanlar travertine is frequently cut by veins of varying thickness (a few cm up to 10 cm) that propagate upward and lateral (Fig. 3d). The contacts between the host rock and veins are intensely deformed and even brecciated. The breccias are angular-shaped, poorly sorted and moderately oriented and set in a matrix composing of iron oxide-rich fine grained material broken off from the host travertine (Fig. 3d).

4.2. Mineralogy of travertine veins

XRD analysis indicates that all carbonate samples are composed chiefly of calcite with minor aragonite (only in sample AK-2T) (electronic appendix). In thin section, euhedral-subhedral calcites are well

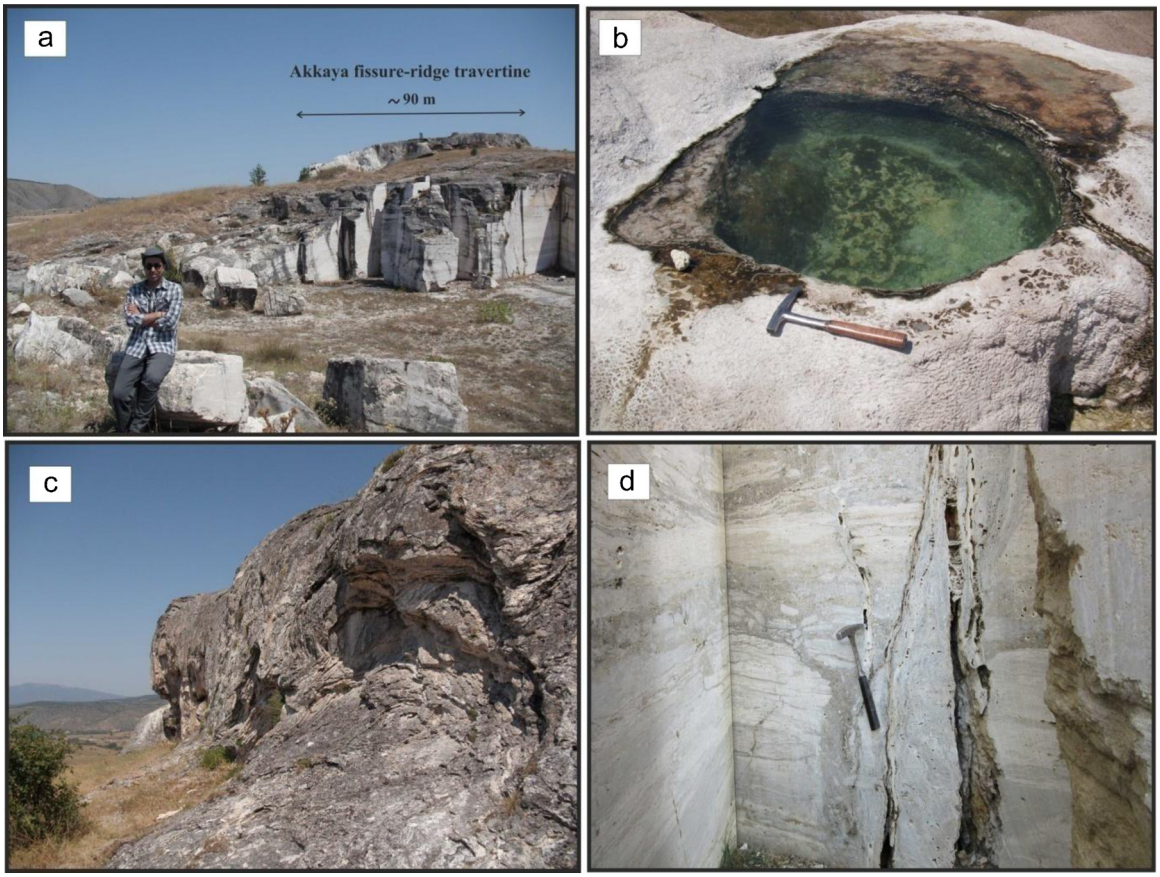

Fig. 3. a) General view of Akkaya fissure-ridge travertine and bedded travertine with vein injections. (arrow direction is close to the north), b) one of the bubbling hot springs on the Akkaya fissure-ridge travertine, c) crystalline crusts on the cascades of Akkaya travertine mound, d) Imanlar bedded travertines with typical breccia zones and injection veins.

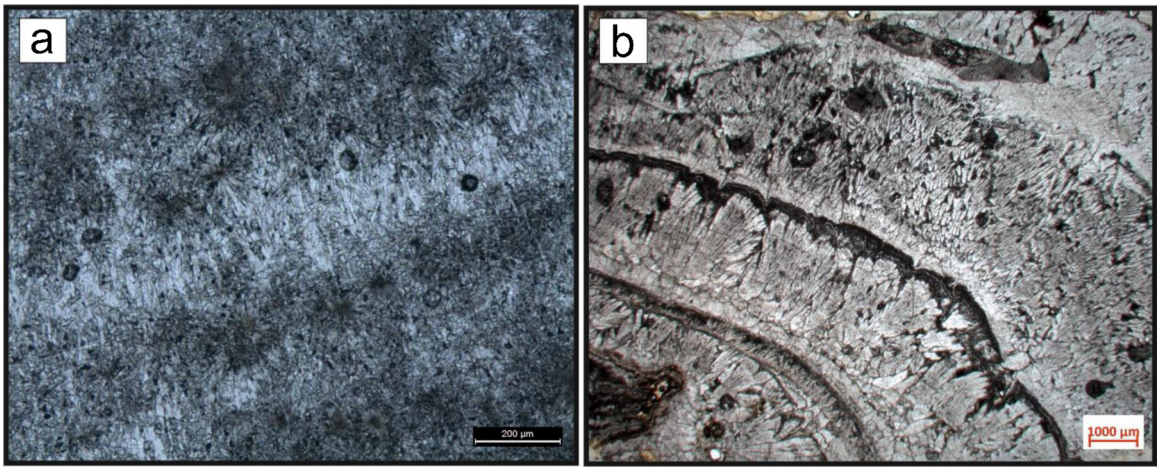

Fig. 4. Thin section micrographs (single nicol) showing a) needle-shaped elongated aragonite + calcite crystals (sample AK-2T) and b) calcite bands (sample IM-D6) confined by thin organic material.

locked and mostly represented by banded texture and width of banding ranges from 0.25 to 2 mm (Fig. 4a, b). Calcites consist of finely crystalline, radial, needle-shaped crystals with a length of up to 0.5 mm. Calcite bands are confined by thin organic material. Aragonites in sample AK-2T are uncolored and noticeable with rod-like or filamentous appearance (Fig. 4a). Raman spectroscopy analysis carried out on a limited number of samples indicated the presence of secondary ankerite on the calcite crystal surface.

The type of carbonate minerals in travertines varies with respect to chemical composition, temperature and carbon dioxide content as well. The aragonite which is less stable than calcite under ambient conditions is very common for travertines precipitating from hot springs (e.g. Rodríguez-Berriguete et al., 2012; Rodríguez-Berriguete and Alonso-Zarza, 2019). Laboratory experiments showed that aragonite crystallizes at temperatures between 30 and 60 °C and it precipitates at low temperature only from waters with high Mg concentration (Pentecost, 2005). According to Jones (2017a), variations in calcite crystal morphogenesis is due to physical and chemical parameters of the parent

Table 1
U-Th data for Akkaya travertines.

Sample name	U (ppm)	^{232}Th (ppb)	(^{230}Th/^{232}Th)	± 2s	(^{232}Th/^{238}U)	± 2s	(^{230}Th/^{238}U)	± 2s	(^{234}U/^{238}U)	± 2s	Uncorr. Age (ka)	± 2s	Corr. Age (ka)	± 2s	Corr. Initial (^{234}U/^{238}U)	± 2s
AK-YR1a	0.0008	0.19	1.48	0.19	0.08	0.02	0.1246	0.016	0.9057	0.0048	16.18	2.24	9.344	4.39	0.8975	0.0062
AK-YR1b	0.0005	0.05	1.15	0.11	0.03	0.00	0.0334	0.003	1.0595	0.0040	3.49	0.33	1.529	1.07	1.0610	0.0041
AK-1T	0.0006	1.20	0.83	0.04	0.64	0.05	0.5272	0.027	1.2210	0.0051	60.43	4.04	16.273	26.61	1.3954	0.1429
AK-2T	0.0067	0.63	0.96	0.07	0.03	0.00	0.0299	0.002	1.2645	0.0035	2.61	0.19	0.856	0.92	1.2706	0.0046
AK-2C	0.0037	4.82	1.19	0.03	0.43	0.02	0.5063	0.013	1.2229	0.0048	57.21	1.87	29.952	14.30	1.3355	0.0647
AK-2D	0.0013	1.08	0.96	0.05	0.28	0.02	0.2660	0.013	1.2491	0.0049	25.90	1.43	9.029	9.13	1.3119	0.0360
IM-D1	0.0021	0.83	4.24	0.12	0.13	0.01	0.5610	0.016	1.4336	0.0038	52.66	1.86	46.207	3.21	1.5405	0.0250
IM-D2	0.0023	2.02	2.20	0.05	0.29	0.01	0.6414	0.015	1.4061	0.0057	64.21	1.97	49.236	6.46	1.5756	0.0646
IM-D3	0.0010	0.62	2.82	0.12	0.20	0.01	0.5695	0.025	1.3145	0.0034	60.34	3.45	49.329	5.89	1.4161	0.0312
IM-D5	0.0118	8.84	3.26	0.03	0.25	0.00	0.8042	0.007	1.2526	0.0031	106.82	1.61	92.864	5.56	1.3910	0.0342
IM-D6	0.0502	1.60	3.02	0.09	0.01	0.00	0.0318	0.001	1.5527	0.0021	2.25	0.07	1.774	0.25	1.5593	0.0029
IM-D7	0.1358	21.89	4.39	0.03	0.05	0.00	0.2333	0.002	1.1594	0.0014	24.37	0.20	21.108	1.61	1.1753	0.0035
IM-D8	0.0018	1.66	2.59	0.05	0.30	0.01	0.7798	0.014	1.3002	0.0051	95.34	2.68	78.721	7.00	1.4661	0.0526
IM-D9	0.0957	17.14	3.70	0.02	0.06	0.00	0.2185	0.001	1.1635	0.0017	22.57	0.15	18.941	1.79	1.1794	0.0041
IM-D10	0.0011	2.74	1.14	0.04	0.82	0.04	0.9312	0.032	1.3667	0.0053	116.07	6.69	67.146	25.86	1.9478	0.4809

Ratios in parentheses are activity ratios calculated from atomic ratios.
The corrected (Corr.) ages (kyr) were calculated using equation given by Cheng et al. (2000) and using half-lives specified in Clark et al. (2012).
All errors are given at 2-sigma level.

water, the presence of impurities, the addition of organic or inorganic materials to the water, the rate of crystal development and/or the presence of microbes. A recent study by Jones (2017b) states that there is no single universal factor controlling the calcite and aragonite precipitation in the springs. Aragonite, generally with calcite as a co-precipitate, is the first phase precipitating from spring waters with high CO_2 content regardless of Mg/Ca ratio. However, aragonite can also be precipitated from waters of low CO_2 content given that Mg/Ca ratio is high enough to inhibit calcite precipitation.

4.3. U-Th age data

^{230}Th/^{232}Th ratios of all the samples are lower than 10 indicating the presence of detrital ^{232}Th (Table 1). The studied travertines are represented by very low U contents (0.5–135.8 ppb). This may show that there might be a time gap between the fissure formation and the initiation of the travertine crystallization which gave rise to debris to accommodate at the deposition site. ^{230}Th/^{232}Th ratios of vein injections (IM labelled) are higher than those of fissure-ridge travertines (AK labelled). Accordingly, the difference between uncorrected and corrected ages of vein injection samples is lower at 2-sigma level (Table 1) which might be attributed to their less porous texture and their relatively higher ^{232}Th content.

U-Th dating results of fissure-ridge travertines and vein injections are shown in Table 1. U-Th dates of vein injections vary in a wide range from 1.77 ± 0.2–92.8 ± 5.5 ka. Samples IM-D1 and IM-D2 and IM-D3 (numbered 1, 2 and 3 in Fig. 5a and b) from multiple parallel vein systems of about 1 cm width from a quarry block yielded identical U-Th ages of 46.2 ± 3.2 ka, 49.2 ± 6.4 ka and 49.3 ± 5.8 ka within analytical errors (Table 1). Samples IM-D5 (Fig. 5c) and IM-D6 (Fig. 5d) from another block give the oldest and youngest ages of the whole data set, 92.8 ± 5.5 and 1.77 ± 0.2 ka, respectively. Four samples taken from a cross-cutting vein system from another travertine block are represented by multiple ages (Fig. 5e). For example, sample IM-D8 dated at 78.2 ± 6.9 ka yields the oldest event. A vertical vein (sample IM-D10) with age of 67.1 ± 25.8 ka is cut by a horizontal vein with ages of 21.1 ± 1.6 ka (sample IM-D7) and 18.9 ± 1.79 ka (sample IM-D9).

The probability distribution of U-Th ages of Akkaya samples is displayed in Fig. 6 which incorporates the 2-sigma range of each date. We observe that travertine precipitation is intensified at 4 major periods, 1.8, 20, 47 and 88 ka. In a previous study, Gökten et al. (2011) presented the first U-Th ages on travertines along the NAFZ. Travertine deposits in the Yeniçağ and Çepni areas, on the main strand of NAFZ in Bolu, are dated 52.7–96.3 ka and 17.9–18.9 ka, respectively. Our unpublished U-Th ages for the Çepni travertines that fall in the range of 79–111 ka are much older than those of Gökten et al. (2011).

U-Th dates of fissure-ridge travertine are younger than those of vein injections and range from 0.85 ± 0.9 ka to 29.9 ± 14.3 ka (Table 1). Samples AK-YR1a and AK-YR1b collected from the eastern and western flanks of the central fissure, respectively (Fig. 7a), yield U-Th ages of 9.34 ± 4.38 ka and 1.52 ± 1.0 ka. Crystalline crusts (samples AK-1T, AK-2T and AK-2D) over this fissure (Fig. 7b–d) are dated 16.2 ± 26.6 ka, 0.85 ± 0.9 ka and 9.02 ± 9.1 ka. One sample from the perched slope (AK-2C) (Fig. 7e) gives an age of 29.9 ± 14.3 ka. Some of U-Th dates of fissure-ridge travertines are contemporaneous with vein injections.

4.4. Rare earth element geochemistry

Total rare earth + Y (REY) contents of samples vary within a wide range from 45 to 131 ppb for fissure-ridge travertines and from 124 to 1027 ppb for vein injections (Table 2). It is obvious that vein injections are represented by higher REY contents than the fissure-ridge travertines. However, REY patterns of both travertine sets are almost 2–5 orders of magnitude lower than the PAAS values (Post-Archean Australian Shale: Taylor and Mclennan, 1985) (Fig. 8). REY concentrations of travertines steeply descend from La to Pr and then sharply ascend from Nd to Eu and continue with a nearly flat pattern across the HREEs. Concentrations steeply ascend from Ho to Y and maintain a horizontal position all the way to Lu. Yttrium anomalies recognized in samples possibly indicate replacement of calcium by this element (e.g. Rankama and Sahama, 1950).

In the same diagram, rare earth element concentrations of studied travertines are compared to those of source lithologies. Total REY contents of Arkot Dağ Complex (Göncüoğlu et al., 2014) and Galatian volcanites (Wilson et al., 1997) are reported 62–158 ppm and 97–489 ppm, respectively. It is shown that REY concentration ranges of host rocks are about 4 orders of magnitude higher than travertines. It is also noticeable that studied travertines have a significant positive yttrium anomaly. REY patterns of Pamukkale vein travertines in western Anatolia (Uysal et al., 2007) are also plotted for comparison (Fig. 8). It is noticeable that trace element contents of travertines from both regions are quite consistent.

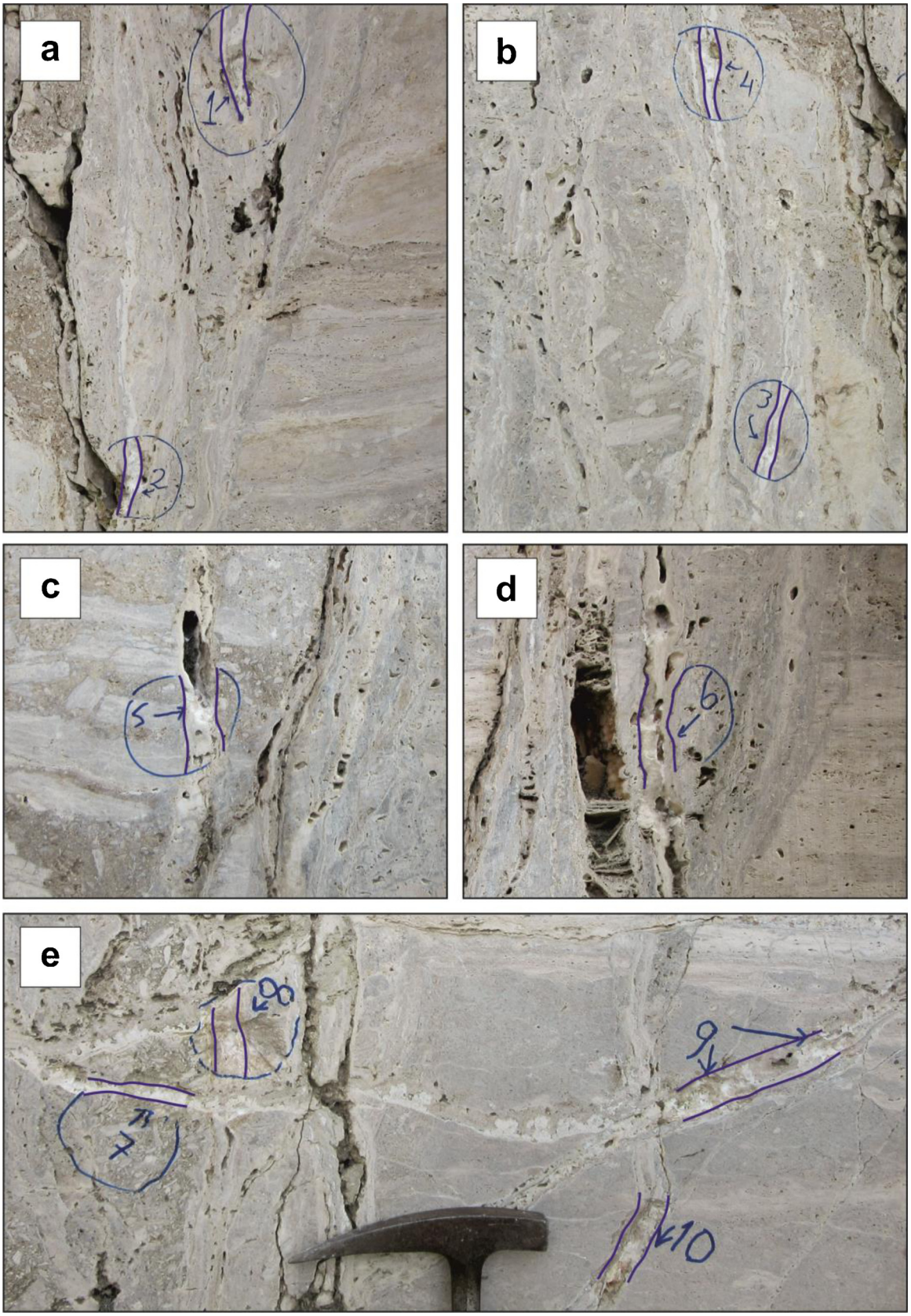

Fig. 5. Images of Imanlar bedded travertine vein samples from a quarry block used for U-series dating. a) Samples IM-D1 and IM-D2 (numbered 1 and 2) b) Samples IM-D3 and IM-D4 represent parallel vein systems of about 1 cm width propagating upward, c) Samples IM-D5 and d) IM-D6 from another block yield the oldest (92.8 ka) and youngest (1.8 ka) ages, respectively, e) Four samples from a cross-cutting vein system (IM-D7, IM-D8, IM-D9 and IM-D10) from a neighboring travertine block are represented by multiple ages.

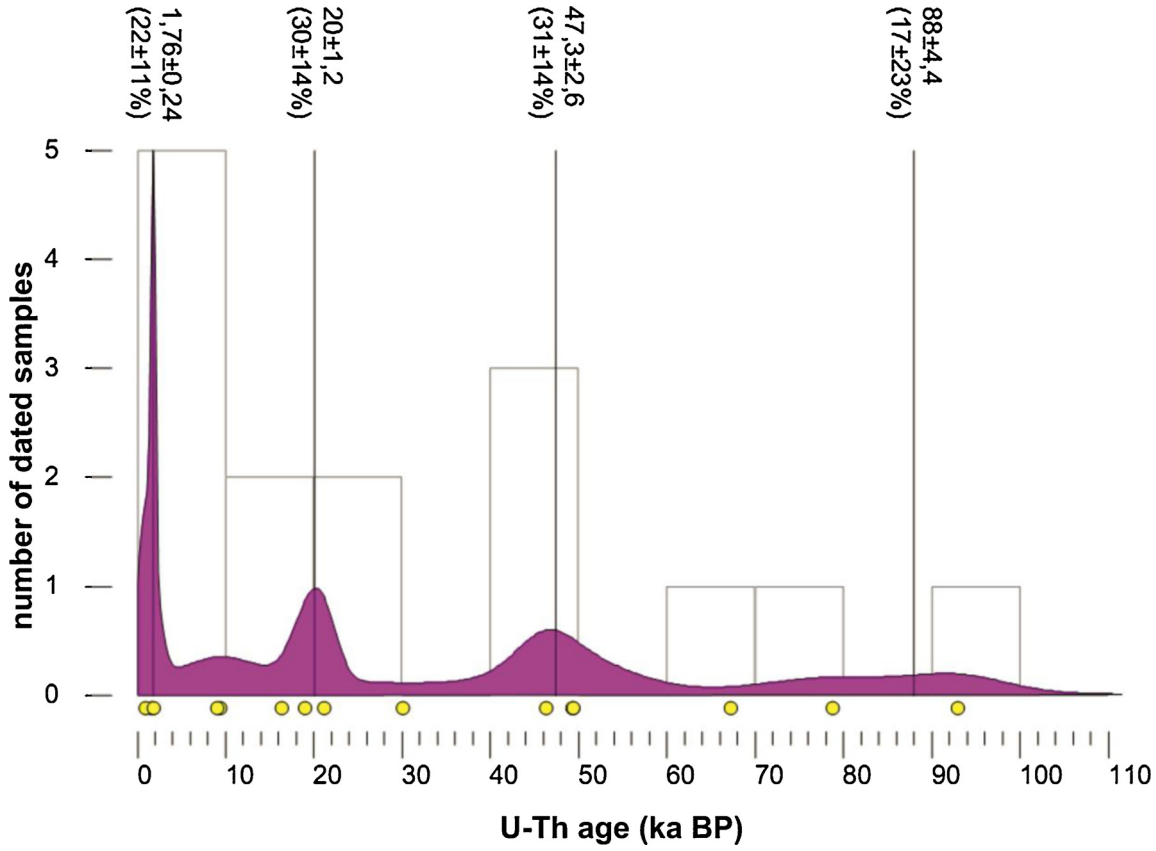

Fig. 6. Relative probability plot and histogram for U-series ages of Akkaya travertine samples.

4.5. Stable isotope data

$\delta^{18}O$ and $\delta^{13}C$ values of studied travertines are given in Table 3. Carbon isotope compositions of fissure-ridge travertines (samples labelled AK) vary from 4.66 to 8.68‰ (VPDB) and those of vein-type travertines (samples labelled IM) range from 4.80 to 7.97‰ (VPDB). Oxygen isotope values of fissure-ridge travertines and vein injections are −15.86 to −7.67‰ and −13.79 to −10.89‰ (VPDB), respectively (Table 3). Results indicated that carbon-oxygen isotope systematics of both travertines span in a similar range. $\delta^{13}C$(DIC) values of thermal water at the Akkaya travertine site vary from 1.19 to 3.01‰ (VPDB) (Ekemen-Keskin, 2010). These values are about 3.5–5.7‰ lower than those of travertines.

4.6. Sr isotope data

Sr isotope compositions Akkaya travertines are shown in Table 3. $^{87}Sr/^{86}Sr$ ratios of fissure-ridge and vein-type travertines are 0.707358 to 0.707406 and 0.707336 to 0.707410, respectively. These values, within analytical error, are quite similar. $^{87}Sr/^{86}Sr$ ratios of Arkot Dağ Complex range from 0.707493 to 0.709032 (Göncüoğlu et al., 2014) and those of Galatian volcanites vary from 0.703450 to 0.706088 (Wilson et al., 1997) (Table 3). In the 1/Sr vs. $^{87}Sr/^{86}Sr$ diagram (Fig. 9), travertines with a wide Sr content but narrow $^{87}Sr/^{86}Sr$ ratios are found to extend between Arkot Dağ Complex and Galatian volcanites. Owing to very close Sr isotope systematics of Akkaya travertines and possible source rocks, it can be argued that Sr in travertines might be derived from the mixing between these two source rocks.

$^{87}Sr/^{86}Sr$ values of Upper Cretaceous seawater are reported in the range of 0.70735 to 0.70770 (Veizer and Compston, 1974). Therefore, the Late Cretaceous marine limestones within the Arkot Dağ Complex could be an alternative source for the observed Sr isotope compositions of travertines (0.707336 to 0.707410).

4.7. Noble gas compositions

To examine the noble gas compositions of fluids that precipitated the travertines at the Akkaya site, two gas and two water samples were collected from bubbling pools (AK1 and AK2). The R/R_A values (where R = sample $^3He/^4He$ and R_A = air $^3He/^4He$) of dissolved gases (sampled from water) are 0.96 and 0.97 and those of free gases are 0.86 and 1.00 (Table 4). The air-corrected $^3He/^4He$ ratios of the same samples (notated by R_A) are slightly lower; 0.42 and 0.84 R_A for dissolved gases and 0.68 and 0.99 R_A for free gases. The difference between measured and air-corrected $^3He/^4He$ values is very small for AK1 gas (0.01 R_A) and water (0.13 R_A) samples. Samples with $^4He/^{20}Ne < 0.318$ (or 0.285 in case of ASW) have probably undergone a diffusive loss of helium which resulted in fractionation of this ratio (e.g. Burnard, 2004; Füri et al., 2010) (Fig. 10).

The corrected $^3He/^4He$ ratios of Akkaya samples are from 0.42 to ~1 R_A and $^4He/^{20}Ne$ ratios are between 0.33 and 0.63. These values are close to the theoretical values of atmosphere and ASW [$^3He/^4He = 1\ R/R_A$, $^4He/^{20}Ne = 0.318$ (air) and $^4He/^{20}Ne = 0.285$ (ASW at Standard Temperature and Pressure)] implying that fluids which precipitated these travertines contain dissolved gases of atmospheric-like composition. Therefore, samples with $^4He/^{20}Ne$ ratios slightly exceeding AIR and ASW values result from a low extent of fractionation of air component.

5. Discussion

5.1. Implications on the regional tectonics

Accumulated strain on fault planes produces earthquakes and under suitable conditions the rupture planes reach the surface along the principal strand of the fault. However, in some cases, deformation could be distributed partially or even entirely in a wide zone on the surface

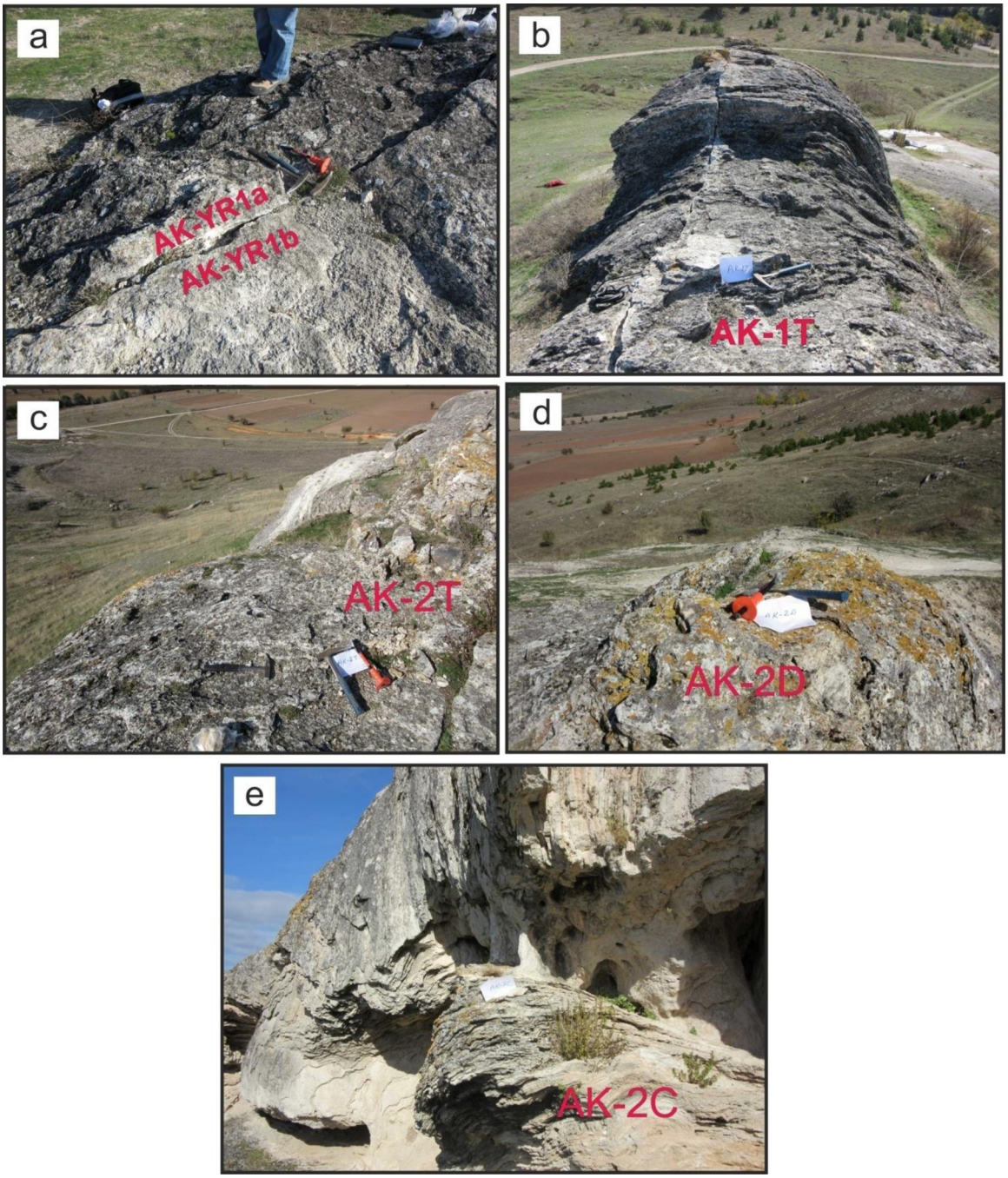

Fig. 7. Images of Akkaya fissure-ridge travertines, a) samples AK-YR1a and AK-YR1b from eastern and western flank of the central fissure; b, c, d) crystalline crusts (samples AK-1T, AK-2T and AK-2D) over the central fissure, e) sample on the cascade of Akkaya travertine (AK-2C).

(Ramsay and Graham, 1970; Ramsay, 1980) as cleavage/boudinage development, granular flow, folding, secondary faulting, pressure solution, microcracking and shifted/deformed veins (McClymont et al., 2009; Titus et al., 2011; Herbert et al., 2014; Kaduri et al., 2019). Therefore, it is crucial to understand the spatial distribution characteristics of the deformation in a shear zone for evaluating the seismic hazard in the surrounding regions.

The Holocene deformation of the west-central NAFZ has long been known around the study area. For example, this section experienced surface faulting during the 1944 Bolu-Gerede (Ms = 7.3) earthquake (Fig. 1a). In the following 6 yrs, the fault at the same site apparently manifested aseismic surface slip before rupturing again during the 1951 earthquake (Ambraseys, 1970; Barka, 1996; Şaroğlu et al., 1992). Following these catastrophic 1944 and 1951 earthquakes, western segments of the NAFZ have received substantial attention by means of seismological trenching for the recognition of paleo-earthquakes (e.g. Hartleb et al., 2006; Kondo et al., 2010; Çağlayan et al., 2019). However, particularly on the northern block there is a wide deformation zone represented by numerous parallel/subparallel faults and the recent behavior and deformation of this zone are not as well documented as the Holocene main fault (i.e. 1944 earthquake rupture).

According to Biryol (2004), slip plane analyses gathered from the syn-depositional shear fractures and growth faults of the latest paleotectonic unit (Eskipazar Formation; Fig. 2) indicated that the study area had experienced a NW–SE directed extension during the Late Miocene–Early Pliocene time interval. Present day neotectonic regime in the

Table 2
REE + Y concentrations of travertine samples (ppb).

Sample no.	La	Ce	Pr	Nd	Sm	Eu	Gd	Tb	Dy	Ho	Y	Er	Tm	Yb	Lu	Total REY
AK-YR1a	6.2	3.7	0.4	2.3	2.2	1.6	0.6	0.1	0.6	0.1	25.3	0.7	0.1	1.3	0.3	45.5
AK-YR1b	4.7	1.4	0.2	1.6	1.9	–	0.2	0.1	0.7	0.3	48.2	1.5	0.3	1.9	0.4	63.4
AK-1B	17.5	11.0	1.3	5.3	4.0	–	0.6	0.1	0.6	0.2	24.0	0.6	0.1	0.6	0.1	66.0
AK-1T	13.8	13.0	1.7	5.4	3.3	–	1.7	0.2	2.0	0.4	32.3	1.2	0.2	1.5	0.2	76.9
AK-2B	12.1	6.3	0.2	2.3	3.4	–	0.2	0.0	0.5	0.1	32.8	0.7	0.2	1.2	0.2	60.2
AK-2C	27.9	36.9	4.6	19.5	5.5	–	2.7	0.4	2.7	0.3	28.2	1.2	0.2	0.9	0.2	131.2
AK-2D	12.1	8.1	1.0	4.6	2.2	–	1.0	0.1	0.4	0.2	43.2	1.2	0.3	2.4	0.4	77.2
AK-2T	9.0	5.7	0.8	3.3	2.5	–	0.6	0.0	0.6	0.1	20.9	0.4	0.2	0.7	0.2	45.0
İM-D1	15.8	12.7	2.1	12.4	5.9	–	13.5	2.8	22.6	7.5	582.1	26.6	4.0	24.4	3.8	736.2
İM-D2	21.7	24.9	3.7	21.3	8.1	–	17.1	3.9	33.1	10.2	800.6	35.9	5.8	36.1	5.1	1027.5
İM-D3	10.2	7.5	0.8	5.6	3.6	–	3.8	0.7	8.2	3.1	289.5	12.5	2.2	16.1	2.5	366.3
İM-D4	49.8	84.0	10.8	43.8	11.4	2.4	13.0	1.9	13.9	3.2	216.8	10.7	1.5	9.1	1.4	473.7
İM-D5	23.0	40.4	4.0	16.4	3.9	1.6	5.0	0.7	4.7	1.5	95.0	4.1	0.7	4.8	0.7	206.5
İM-D6	17.6	21.3	2.1	10.4	5.0	–	2.5	0.6	4.1	0.7	53.2	2.8	0.5	3.1	0.5	124.4
İM-D7	132.5	277.7	29.0	108.5	21.6	5.6	21.1	3.4	20.1	4.6	197.6	13.4	2.1	15.2	2.2	854.6
İM-D8	27.3	14.1	2.6	15.1	8.2	–	9.4	1.8	11.7	3.8	288.1	14.4	2.0	14.9	2.2	415.6
İM-D9	57.5	100.8	13.8	50.4	11.3	3.8	10.2	1.6	10.0	1.9	89.8	5.1	0.8	4.9	0.6	362.5
İM-D10	15.4	17.2	2.1	9.6	3.8	2.3	3.6	0.6	5.3	1.6	133.4	5.7	0.9	5.1	0.8	207.4

region is represented by a NNW-SSE-trending S_{Hmax} axis (the World Stress Map Project database; Heidbach et al., 2016). Moreover, results of the lineament analysis from the LandsatETM images imply that the study area has been controlled by a NW–SE trending compression (Kuterdem, 2005) which is in good agreement with major fault geometries that we mapped in the distributed deformation zone.

Hot springs and travertine precipitation are very clear evidences of the ongoing activity of the Akkaya fissure-ridge. The fissure-ridge travertine occurs along the ~NNW-striking dilation fracture (Fig. 1b). The main vein is solid itself and there are secondary fissures parallel/subparallel to the local S_{Hmax} direction (N35-40W) (Fig. 1b). Thus, it is concluded that the Akkaya fissure-ridge is in favor of the regional horizontal compressional stress axis.

5.2. Fluid source

5.2.1. Significance of stable isotope data

Waters issuing from hot springs at the northern part of the Akkaya fissure-ridge travertine (Fig. 3b) have TDS values up to 2260 mg/l and temperature of 36 °C (Ekemen-Keskin, 2010). Ca and HCO_3 concentrations of these waters are reported to be 212 and 3124 mg/l, respectively. Using these chemistry data and the PHREEQC aqueous speciation software (Parkhurst and Appelo, 2013), we calculated the saturation state of Akkaya thermal water with respect to carbonate minerals. Results of mineral equilibrium computations revealed saturation of both calcite and aragonite in this water, however, degree of saturation is higher for the former.

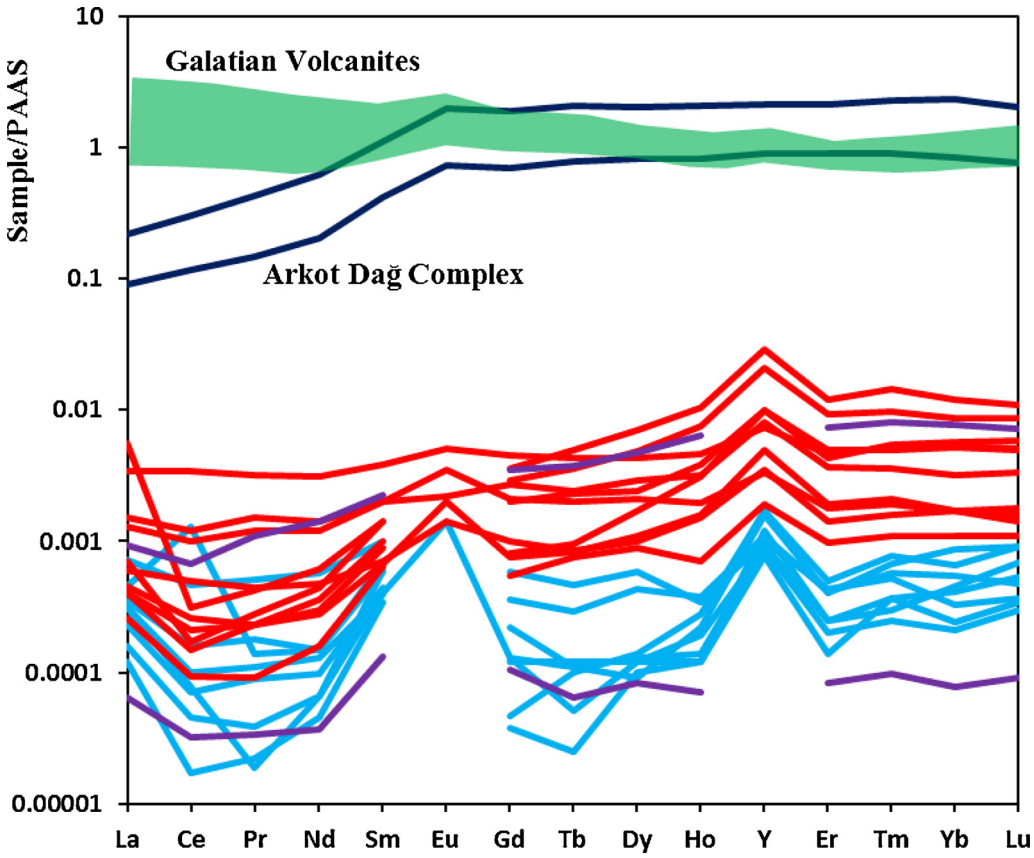

Fig. 8. REE + Y concentrations of travertines and host rock samples. Red and blue lines correspond to vein injections and fissure-ridge travertines, respectively. Data on Arkot Dağ Complex, Galatian volcanites and Pamukkale travertines (purple lines) are from Göncüoğlu et al. (2014); Wilson et al. (1997) and Uysal et al. (2007). PAAS-normalized values are from Taylor and Mclennan (1985).

Table 3
Stable (‰) and Sr isotope compositions of travertines and host rocks.

Lithology	Sample no.	$\delta^{13}C$ (VPDB)	$\delta^{18}O$ (VPDB)	$\delta^{18}O$ (VSMOW)	$^{87}Sr/^{86}Sr$	± 2σ	Sr (ppm)
Akkaya travertines	AK-YR1a	4.66	−15.86	14.51	0.707406	0.000011	1351
	AK-YR1b	4.75	−15.47	14.91	0.707378	0.000010	1344
	AK-1B	6.78	−11.97	18.52	n.a	n.a	3436
	AK-1T	6.29	−13.24	17.21	0.707387	0.000010	2182
	AK-2B	6.20	−13.11	17.34	0.707405	0.000010	3273
	AK-2C	8.68	−7.67	22.95	0.707367	0.000009	3804
	AK-2D	5.56	−14.36	16.06	0.707358	0.000010	1693
	AK-2T	5.70	−13.63	16.81	0.707365	0.000009	2622
	IM-D1	4.80	−13.70	16.74	0.707407	0.000010	1736
	IM-D2	4.83	−13.79	16.64	0.707410	0.000010	1873
	IM-D3	4.80	−13.32	17.13	0.707397	0.000009	1776
	IM-D4	5.32	−13.28	17.17	0.707409	0.000011	1301
	IM-D5	5.58	−12.08	18.41	0.707372	0.000011	1530
	IM-D6	7.01	−10.89	19.63	0.707336	0.000011	1993
	IM-D7	7.78	−11.98	18.51	0.707403	0.000011	2223
	IM-D8	5.50	−11.24	19.27	0.707380	0.000009	1904
	IM-D9	7.97	−12.48	17.99	0.707404	0.000010	2764
	IM-D10	5.73	−11.49	19.01	0.707393	0.000013	1214
Arkot Dağ Complex	Gü395				0.706088		466
	Gü486				0.703450		694
	Gü490				0.705290		1261
	Gü512				0.705630		684
	Gü395				0.706088		466
	Or29				0.704580		842
	Or28				0.705130		739
	Ky2				0.704534		617
Galatian volcanites	UKF5				0.709032		192
	UKF6				0.707493		144
	UKF7				0.707559		179
	UKF8				0.707686		201
	UKF15				0.707617		149

$^{87}Sr/^{86}Sr$ ratios of Arkot Dağ Complex and Galatian volcanites are from Göncüoğlu et al. (2014) and Wilson et al. (1997), respectively.

Carbon isotope compositions of samples varying from 4.66 to 8.68‰ (VPDB) yield similar ranges for fissure-ridge and vein-type travertines. These values are higher than the array proposed for the marine limestones (Clark and Fritz, 1997) but consistent with carbon isotope composition of meteogene fluids (typically –3 to +8‰; Pentecost, 2005). However, $\delta^{13}C$ values measured on dissolved inorganic carbon (DIC) of Akkaya thermal spring are significantly lower and span from 1.19 to 6.3‰ (average 3.36‰) (Ekemen-Keskin, 2010) falling in the range of limestones. Heavy-carbon enrichment in travertines might be explained by preferential separation of ^{13}C (volatilization) from fluids interacting with carbonate rocks (decarbonatization reaction). Such ^{13}C-enriched CO_2 dissolves in thermal water at depth and precipitates travertines at near surface (e.g. Uysal et al., 2009). Because carbon isotopes are considerably fractionated from the original compositions, they may not yield reliable information for the CO_2 source.

Degassing of CO_2, which induces $CaCO_3$ formation, results in fractionation of C isotopes. Accordingly, the residual DIC and the

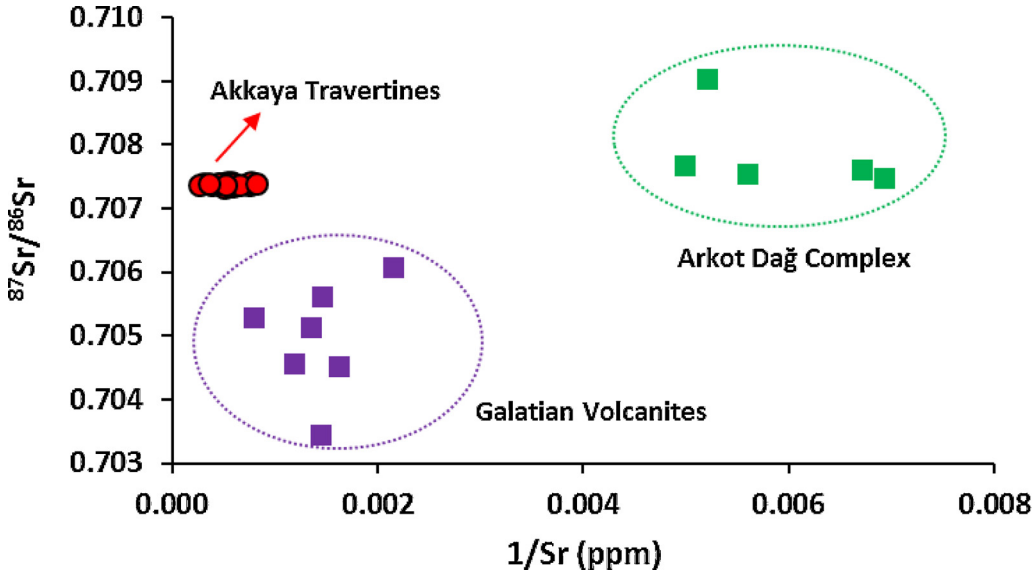

Fig. 9. 1/Sr vs. $^{87}Sr/^{86}Sr$ diagram for the travertine samples. Data on Arkot Dağ Complex are from Göncüoğlu et al. (2014) and Galatian volcanites from Wilson et al. (1997).

Table 4
Noble gas compositions of Akkaya thermal waters.

Sample no	Sample Type	Temp. (°C)	pH	R/R_a	R/R_a (corr.)	± 2σ	He/Ne	He cc/l	Ne cc/l	^{40}Ar ppm	^{40}Ar ± 2σ	^{38}Ar ppm	^{38}Ar ± 2σ	^{36}Ar ppm	^{36}Ar ± 2σ	$^{40}Ar/^{36}Ar$ (corr.)	± 2σ	$^{38}Ar/^{36}Ar$ (corr.)	± 2σ
AK1	Water	24	6.5	0.97	0.84	0.013	0.36	$3.4.10^{-5}$	$9.59.10^{-5}$	2379	5.82	1.53	$4.4.10^{-3}$	8.154	$2.2.10^{-2}$	292.2	0.109	0.1872	0.000295
AK1	gas	24	6.5	1	0.99	0.006	0.39	0.05	0.12	96	0.025	0.06	$8.7.10^{-5}$	0.33	$1.5.10^{-4}$	290.2	0.112	0.1864	0.000259
AK2	Water	19	6.8	0.96	0.42	0.007	0.31	$3.4.10^{-5}$	$1.15.10^{-4}$	3703	9.043	2.38	$6.4.10^{-3}$	12.69	$3.4.10^{-2}$	292.3	0.082	0.1875	0.000206
AK2	gas	19	6.8	0.86	0.68	0.022	0.57	0.11	0.2	240	0.107	0.15	$1.2.10^{-4}$	0.825	$5.1.10^{-4}$	291	0.075	0.1876	0.000124

precipitated calcite are enriched in heavy carbon isotope (^{13}C) due to preferential loss of ^{12}C. In conclusion, travertine formed by CO_2 degassing can get significantly enriched in ^{13}C as found in the present study.

In the $\delta^{13}C$ vs. $\delta^{18}O$ diagram (Fig. 11), fissure-ridge ($r^2 = 0.98$) and vein-type travertines ($r^2 = 0.71$; excluding two samples) define a very strong positive correlation. The diagram indicates that heavy isotope enrichment is not limited only to carbon but also oxygen isotopes. It was shown that during rapid (non-equilibrium) CO_2 degassing triggered by seismic events, deposited travertines would be enriched in both ^{18}O and ^{13}C (e.g. Pentecost, 2005). Zheng (1990) suggested that the positive correlation between $\delta^{13}C$ and $\delta^{18}O$ values of travertines is attributed either to the precipitation of calcite from a H_2CO_3-dominant fluid accompanied by a progressive decrease in temperature during CO_2 degassing or boiling of HCO_3-dominant water. Nearly neutral pH values (6.64–7.04) of Akkaya thermal water exclude the possibility of precipitation from H_2CO_3-dominant water.

Alternatively, Ren et al. (2015) proposed that the positive correlation between carbon and oxygen systematics of calcites can be explained by two processes: mixing of two fluids with diverse isotopic compositions or the calcite precipitation, which is due to a temperature change coupled with either CO_2 degassing or fluid/rock interaction. If mixing had been the major process responsible for calcite precipitation, there would be different fluids with distinct isotopic compositions and temperatures. However, carbon and oxygen compositions of travertine samples do not support this mechanism. Indeed, CO_2 degassing is shown to be the principal mechanism for the travertine formation (e.g. Uysal et al., 2007, 2009; Karabacak et al., 2017).

To test this, oxygen isotope composition of fluid/s that precipitated the travertines is estimated. Oxygen isotope values of studied travertines are 14.51–22.95‰ (VSMOW). $\delta^{18}O$ of the thermal spring at Akkaya varies in a narrow range from −12.35 to −12.06‰ (VSMOW) (Ekemen-Keskin, 2010) which are lower than oxygen isotope values of travertines. Using the oxygen isotope fractionation between calcite and water ($\Delta^{18}O_{calcite\text{-}water}$) proposed by Friedman and O'Neil (1977) and assigning a fluid temperature of 36 °C (the measured temperature of the Akkaya spring), the $\delta^{18}O$ of fluid equilibrating with the studied travertines was computed in the range of -11.6 to -3.2‰ (average −8.7‰) which evidently points to a meteoric origin. Owing to that fractionation equation of Friedman and O'Neil (1977) might underestimate the oxygen fractionation, we used equations of Coplen (2007) and Kele et al. (2015) to recalculate $\delta^{18}O$ of fluid. Results from the respective equations revealed $\delta^{18}O$ values in the range of −13.1 to −4.7‰ (average −10.2‰) and -14.1 to -5.7‰ (average −11.2‰). These values are nearly 1.5–2.5‰ negative than those estimated by the Friedman and O'Neil's (1977) equation. Supposing that discharge temperature of Akkaya spring has not considerably changed in the studied time interval, estimated $\delta^{18}O_{water}$ values are quite consistent with the average value (−12.3‰) reported by Ekemen-Keskin (2010).

Another attempt was made here to compute the temperature of paleo-fluid(s) which precipitated the Akkaya travertines. In the calculations, we used $\delta^{18}O$ of travertines and Akkaya spring water. Temperatures estimated using the Coplen's (2007) equation vary from 19.7 to 40.9 °C (average 31.9 °C) for the fissure-ridge travertines and from 14.3 to 29.2 °C (average 22.1 °C) for the vein travertines. The equation of Kele et al. (2015) yielded notably higher results with ranges of 26.2–45.3 °C (average 37.2 °C) and 21.3–34.8 °C (average 28.4 °C) for the respective travertines. Fluid temperatures computed by the equation of Kele et al. (2015), particularly for the vein travertines, show an excellent fit with the measured temperature of Akkaya spring water (36 °C). This might imply that there was no significant change in the temperature of Akkaya spring through time.

5.2.2. Sr and REY compositions

Sr concentrations of travertines are in the range of 1344–3804 ppm (average 2463 ppm) for the fissure-ridge travertines and

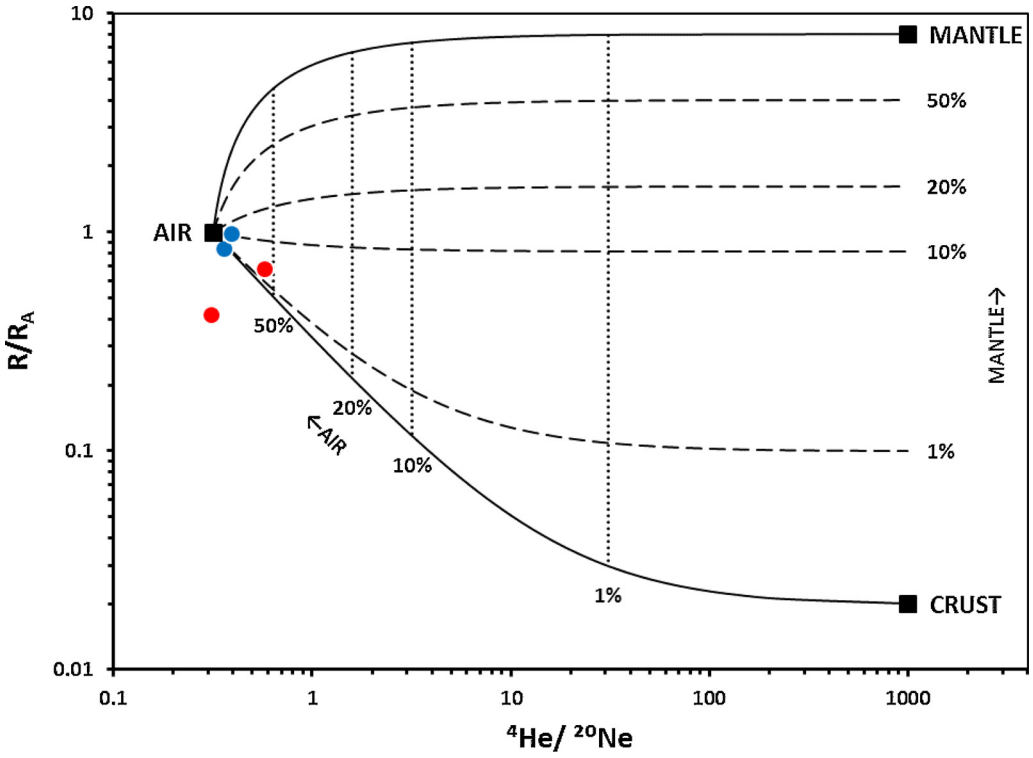

Fig. 10. $^{4}He/^{20}Ne$ vs. R/R_A diagram for the gas and spring samples at the Akkaya site. Blue is sample AK-1 and red is sample AK-2.

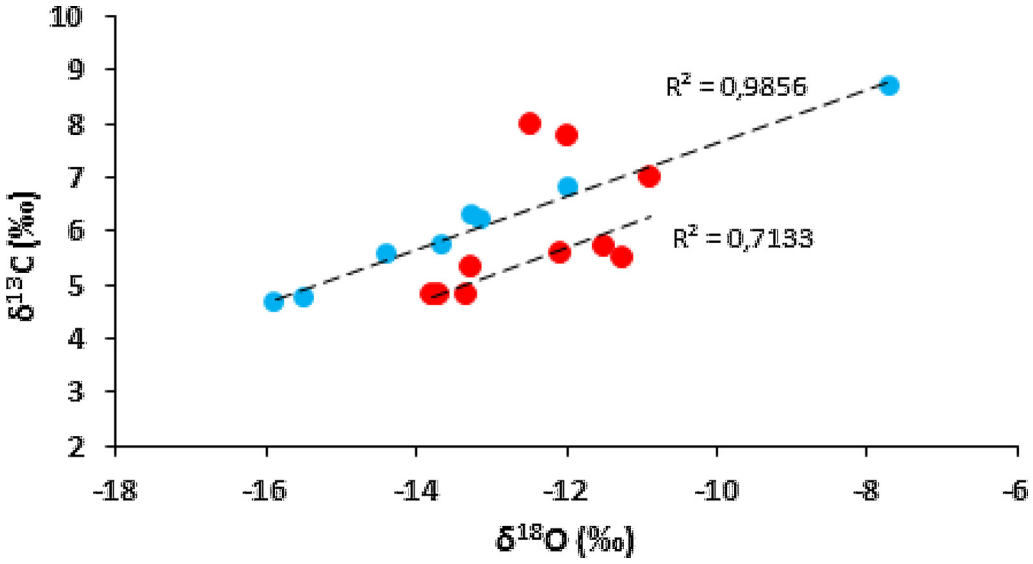

Fig. 11. $\delta^{13}C$ vs. $\delta^{18}O$ diagram for travertine samples. Red and blue circles correspond to vein injections and fissure-ridge travertines, respectively.

1213–2763 ppm (average 1831 ppm) for the vein-type travertines. Galatian volcanites and mafic rocks of Arkot Dağ Complex (basalt) have Sr contents of 466–1261 ppm (Wilson et al., 1997) and 144–200 ppm (Göncüoğlu et al., 2014) which are much lower than those of travertines. High Sr concentration of travertines is most probably due to replacement of Ca by Sr in calcite/aragonite structure since these two elements behave in a similar manner as their ionic radius are very similar and both occur in divalent oxidation state. Although Sr isotope compositions of travertines are within the range of host rocks, their REY contents are significantly low (Fig. 9). This might be attributed to the fact that during water-rock interaction isotopes of high atomic mass, like Sr, are not significantly fractionated whereas trace elements concentrations are notably affected by element uptake and loss (e.g., Banner, 1995; Rimstidt et al., 1998).

Although REEs behave in a more compatible manner in calcite (with a total partition coefficient of log D_{REE} = 4.4; Tanaka and Kawabe, 2006) than in magmatic minerals (log D_{REE} = 0.9–1.6; Rollinson, 1993), rare earth element concentrations of fissure-ridge and vein-type travertines are noticeably low (Fig. 8). REE data might indicate rapid ascent of CO_2-bearing fluids without sufficient interaction with the host rocks (e.g. Uysal et al., 2009). Thermal waters issuing along the 1944 earthquake rupture of the NAFZ are reported to have very high HCO_3 contents (from 4906 to 6809 mg/l; Süer et al., 2008) and $CO_2/^3He$ ratios ($> 5 \times 10^{14}$; de Leeuw et al., 2010). Ekemen-Keskin (2010) measured 660 mg/l dissolved CO_2 in the Akkaya thermal spring. The retardation of chemical reactions during the water-rock interaction by

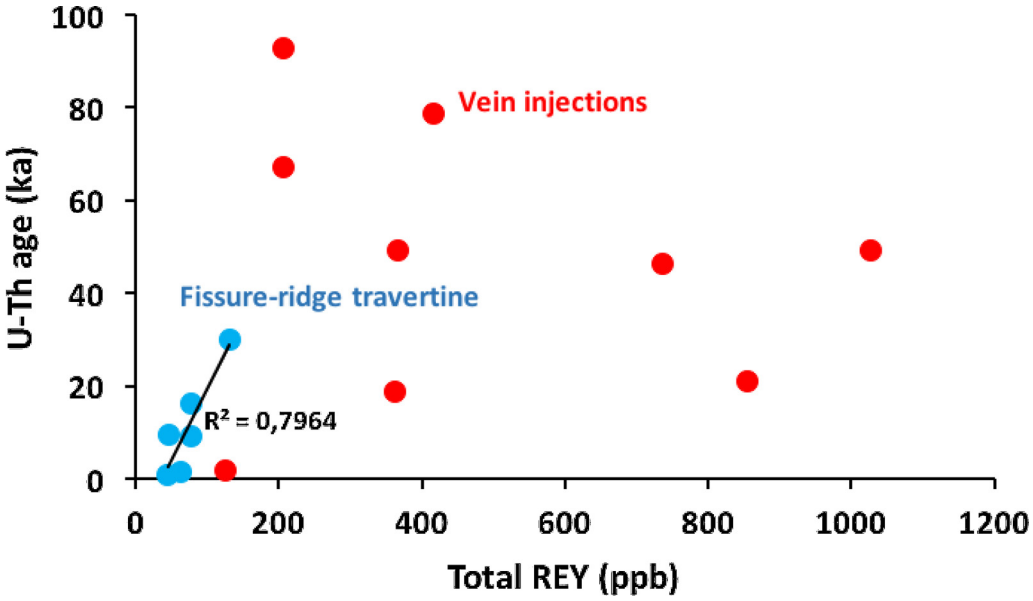

Fig. 12. U-Th age vs. Total REY diagram.

CO_2-dominated fluids (e.g. Huang and Longo, 1994; Uysal et al., 2009) or retention of REY by the alteration minerals (clays) (Möller et al., 2003) may well explain the low rare earth element concentrations of travertines and the REY patterns inconsistent with those of Arkot Dağ Complex and Galatian volcanites (Fig. 8).

In Fig. 12, temporal changes in REY concentrations of fissure-ridge and vein-type travertines are compared. Regarding fissure-ridge travertines, U-Th ages are significantly positively correlated with REY contents (r^2 = 0.796) indicating limited rock leaching in time. However, vein-type travertines, which are relatively older than fissure-ridge travertines, do not display any temporal correlation with REY concentrations suggesting prolonged water-rock interaction.

5.2.3. Volatile provenance

Variations in helium isotope ($^3He/^4He$) composition can be used as tracers of the effect of crustal and mantle volatiles in different tectonic settings. ^3He has a primordial origin and is still degassing from the mantle. However, ^4He is produced by radioactive decay of U and Th in minerals. Because isotopic compositions of mantle and crust are widely different, helium isotope studies of natural waters in continental regions provide significant information on mantle-derived contributions to crustal fluids and the rate of mantle degassing through the Earth crust (e.g. Hilton et al., 2002).

Since helium is quite insoluble in aqueous solutions it preferentially partitions into the vapor phase in the case of vapor loss, and therefore, the gas samples at Akkaya have slightly higher $^3He/^4He$ values (0.68 to 0.99 R/R_A) than the water samples (0.42 to 0.84 R/R_A). Akkaya samples have $^3He/^4He$ ratios which are significantly greater than values characteristic of radiogenic helium production in crustal lithologies (average R/R_A = 0.05; Farley and Neroda, 1998; Barry et al., 2014). As regards the previous studies on helium isotope compositions of geothermal fluids along the NAFZ, reported $^3He/^4He$ values for the Kurşunlu geothermal site, nearly 30 km east of Akkaya travertines, closely fall within the range of this study (0.85–1.33 R/R_A: Güleç et al., 2002; de Leeuw et al., 2010). Using a simple binary mixing between mantle (8 R/R_A) and crustal (0.05 R/R_A) helium components (Farley and Neroda, 1998), proportion of mantle-derived helium in Akkaya samples (gas phase) is found 8.5–12.3%.

5.3. Constraints on co-seismic vein growth

Pressurized CO_2-rich waters in the subsurface reservoirs are mobilized during sudden crustal strain (Montgomery and Manga, 2003; Wang et al., 2004; Berardi et al., 2016; Karabacak et al., 2017) giving rise to carbonate precipitation within fractures that act as a conduit for the hot waters (Sibson, 1987; Altunel and Karabacak, 2005; Fig. 1a). Most of the previous studies on carbonate veins focus on the active faults and related deformational features (e.g. type and direction of regional stresses, dilatational rate). In recent works, their relation with the repeated seismic releases is also addressed (e.g., Uysal et al., 2007; Mesci et al., 2008; Nuriel et al., 2011; Brogi et al., 2017; Williams et al., 2017). Moreover, it is shown that the age distributions of bands in a carbonate vein provide direct dates of the surrounding major earthquakes (Karabacak et al., 2019). In this study, our dating results on Akkaya travertines imply that crustal deformation is intensified at 4 major periods, 1.8, 20, 47 and 88 ka that could be interpreted as the repeated seismic releases within the NAFZ.

Upward and/or lateral bifurcation of injection-type veins indicates formation by CO_2-rich overpressurized fluids during the seismic unrest (e.g. Uysal et al., 2009). Experimental studies showed that, during propagation of these buoyant fluids to the surface, tensile stress developing at the tip of an overpressured hydrofracture might lead off horizontal and vertical discontinuities to a considerable distance (Gudmundsson and Brenner, 2001; Gudmundsson et al., 2002). Travertine veins in Pamukkale (Uysal et al., 2009) and Marmaris (Ünal–İmer et al., 2016) areas in Turkey are reported to form dyke- and sill-like structures of about 1–3 m high within the early-deposited travertines and host limestone, respectively.

Samples IM-D1, IM-D2 and IM-D3 collected from three parallel vein systems (a few cm across) in a quarry block yielded quite similar ages ranging from 46.2 to 49.3 ka (Fig. 6a). This may indicate that overpressurized fluid opened up subparallel hydrofractures. However, in a neighboring block (Fig. 6b), two calcite veins (Samples IM-D5 and IM-D6) parallel to the main fracture have ages falling between 1.8–92.8 ka implying reign of prolonged seismic activity.

If the stress field along the pathway of fluid is not homogenous, the hydrofracture may then be unable to propagate upward and either is terminated or changes into a T-shaped fracture (Gudmundsson and Brenner, 2001). Fig. 6c shows that the brecciated main vein on another block is branched to a number of crossed, horizontal and even parallel subveins with different crystallization ages. It is important to note that horizontal subveins with identical U-Th ages of 21.1and 18.9 ka most probably formed during the same seismic event. It is likely that occurrence of injection-type veins (brecciated zone) has localized to the

bedded travertine and we did find no evidence of such structures within the fissure-ridge travertine. However, younger age of sample IM-D6 (1.8 ka) might indicate that CO_2 degassing continued through the Holocene time. Although we could not date all the seismic episodes systematically at the Akkaya site, nevertheless, our results point to that the seismic unrest in the area reigned from Late Pleistocene to present.

Our results show that the deformation of NAFZ should not be regarded as a simple recent earthquake rupture and/or creep only along the principal fault strand. Several brittle properties such as parallel/subparallel faults, hydrofractures, microcracking and veins exert a great control on the distributed deformation.

6. Conclusions

In this study new chronological, isotopic and geochemical data are presented for the Akkaya travertine site in northwest Turkey. Because the studied travertines are located in close proximity to the 1944-earthquake rupture of the North Anatolian Fault Zone, U-Th dating results on these carbonates are crucial for the ascertainment of seismic frequency on the west-central part of the NAFZ. The Akkaya travertines consist of two major sequences; the older series is represented by bedded travertines which host a variety of vein injections with a wide range of crystallization age from 1.8 to 93 ka BP and the younger one is comprised by fissure-ridge carbonates with age ranging from 0.8 to 29 ka BP.

$\delta^{18}O$ and $\delta^{13}C$ values of travertines which are lower than those of recent hot springs were fractionated by rapid CO_2 degassing during seismic unrest. $\delta^{18}O$ of the fluids precipitating the Akkaya travertines is found to have a meteoric origin and the paleo-temperature of fluids did not significantly change through the studied time interval. Sr isotope values of Akkaya travertines are quite different from mafic bedrocks and fall in the range of Upper Cretaceous marine limestones. The REY patterns of travertines are significantly lower than source lithologies but consistent with range suggested for the Pamukkale travertines. Helium isotope compositions of gas and thermal fluids in the area yield mantle contribution up to 12 %.

CRediT authorship contribution statement

Gokhan Yıldırım: Data curation, Conceptualization, Software, Methodology, Writing - original draft, Investigation. **Halim Mutlu:** Data curation, Writing - original draft, Supervision, Conceptualization, Formal analysis, Conceptualization, Investigation, Writing - review & editing. **Volkan Karabacak:** Writing - review & editing, Writing - original draft, Formal analysis. **I. Tonguç Uysal:** Investigation, Writing - original draft, Writing - review & editing, Methodology. **Kadir Dirik:** Project administration, Funding acquisition, Resources, Investigation. **Abidin Temel:** Project administration, Funding acquisition, Resources. **Galip Yüce:** Visualization, Validation. **Jian-xin Zhao:** Data curation.

Declaration of Competing Interest

The authors declare that they have no known competing financial interests or personal relationships that could have appeared to influence the work reported in this paper.

Acknowledgements

This study is supported by the Scientific and Technological Research Council of Turkey (TUBITAK) under grant no 114Y544. David Dettman is acknowledged for the stable isotope analyses and Andrea L. Rizzo (INGV, Palermo) for noble gas analyses. Authors are grateful to Kıymet Deniz (Ankara University) for Raman spectroscopy determinations. The appreciation is extended to Álvaro Rodríguez-Berriguete, Martin Dietzel and two anonymous reviewers for their critical comments which greatly improved the manuscript.

Appendix A. Supplementary data

Supplementary material related to this article can be found, in the online version, at doi:https://doi.org/10.1016/j.chemer.2020.125630.

References

Altunel, E., Karabacak, V., 2005. Determination of horizontal extension from fissure-ridge travertines: a case study in the Denizli Basin, southwestern Turkey. Geodin. Acta 18 (3–4), 333–342.
Ambraseys, N.N., 1970. Some characteristic features of the Anatolian fault zone. Tectonophysics 9, 143–165.
Ayhan, M.E., Koçyiğit, A., 2010. Displacements and kinematics of the February 1, 1944 gerede earthquake (North Anatolian fault system, Turkey): geodetic and geological constraints. Turk. J. Earth Sci. 19, 285–311.
Banner, J.L., 1995. Applications of the trace element and isotope geochemistry of strontium to studies of carbonate diagenesis. Sedimentology 45 (2), 805–824.
Barka, A.A., 1996. Slip distribution along the North Anatolian Fault associated with the large earthquakes of the period 1939 to 1967. Bull. Seismol. Soc. Am. 86, 1238–1254.
Barry, P.H., Hilton, D.R., Füri, E., Halldórsson, S.A., Gronvold, K., 2014. Carbon isotope and abundance systematics of Icelandic geothermal gases, fluids and subglacial basalts with implications for mantle plume-related CO_2 fluxes. Geochim. Cosmochim. Acta 134, 74–99.
Berardi, G., Vignaroli, G., Billi, A., Rossetti, F., Soligo, M., Kele, S., et al., 2016. Growth of a Pleistocene giant carbonate vein and nearby thermogene travertine deposits at Semproniano, southern Tuscany, Italy: estimate of CO_2 leakage. Tectonophysics 690, 219–239 0.
Biryol, C.B., 2004. Neotectonics and Evolution of the Eskipazar Basin, Karabük, Turkey. Middle East Technical University, Ankara MSc. Thesis, 124 p.
Bozkurt, E., 2001. Neotectonics of Turkey – a synthesis. Geodin. Acta 14, 3–30.
Brogi, A., Capezzuoli, E., Kele, S., Baykara, M.O., Shen, C.C., 2017. Key travertine tectofacies for neotectonics and palaeoseismicity reconstruction: effects of hydrothermal overpressured fluid injection. J. Geol. Soc. 174 (4), 679–699.
Burnard, P., 2004. Diffusive fractionation of noble gases and helium isotopes during mantle melting. Earth Planet. Sci. Lett. 220, 287–295.
Çağlayan, A., Işık, V., Saber, R., 2019. An assessment of holocene seismic activity on 1944 earthquake segment, North Anatolian Fault Zone (Turkey). Geosci. J. https://doi.org/10.1007/s12303-018-0075-3.
Cheng, H., Edwards, R.L., Hoff, J., Gallup, C.D., Richards, D.A., Asmerom, Y., 2000. The half-lives of uranium-234 and thorium-230. Chem. Geol. 169, 17–33.
Clark, I.D., Fritz, P., 1997. Environmental Isotopes in Hydrogeology. Lewis Publishers, New York, NY, USA.
Coplen, T.B., 2007. Calibration of the calcite–water oxygen-isotope geothermometer at Devils Hole, Nevada, a natural laboratory. Geochim. Cosmochim. Acta 71, 3948–3957.
Cox, S.F., 2007. Structural and isotopic constrains on fluid flow regimes and fluid pathways during upper crustal deformation: an example from the Taemas area of the Lachlan Orogen, SE Australia. J. Geophys. Res. Solid Earth 112 (B8).
D'Alessandro, W., Glammanco, S., Bellomo, S., Parello, F., 2007. Geochemistry and mineralogy of travertine deposits of the SW flank of Mt. Etna (Italy): relationships with past volcanic and degassing activity. J. Volcanol. Geotherm. Res. 165 (1–2), 64–70.
De Leeuw, G.A.M., Hilton, D.R., Güleç, N., Mutlu, H., 2010. Regional and temporal variations in $CO_2/^3He$, $^3He/^4He$ and $\delta^{13}C$ along the North Anatolian Fault Zone, Turkey. Appl. Geochem. 25, 524–539.
Ekemen-Keskin, T., 2010. Groundwater changes in relation to seismic activity: a case study from Eskipazar (Karabük, Turkey). Hydrogeol. J. 18, 1205–1218.
Emre, Ö., Duman, T.Y., Özalp, S., 2011. 1:250000 Scale Active Fault Map Series of Turkey, Bolu (NK 36-14) Quadrangle. Serial Number: 19. General Directorate of Mineral Research and Exploration, Ankara, Turkey.
Farley, K.A., Neroda, E., 1998. Noble gases in the Earth's mantle. Annu. Rev. Earth Planet. Sci. 26, 189–218.
Friedman, I., O'Neil, J.R., 1977. Compilation of Stable Isotope Fractionation Factors of Geochemical Interest. USGS Numbered Series (report), 440- KK, 11 p.. .
Füri, E., Hilton, D.R., Halldórsson, S.A., Barry, P.H., Hahm, D., Fischer, T.P., Grönvold, K., 2010. Apparent decoupling of the He and Ne isotope systematics of the Icelandic mantle: the role of He depletion, melt mixing, degassing fractionation and air interaction. Geochim. Cosmochim. Acta 74, 3307–3332.
Gökten, E., Demirtaş, R., Özaksoy, V., Herece, E., Varol, B., Temiz, U., 2011. Faulting and stress distribution in the Bolu pull e apart basin (North Anatolian fault zone, Turkey): the Significance of New dates obtained from the Basin fill. Turk. J. Earth Sci. 20, 1–26.
Göncüoğlu, M.C., Marroni, M., Pandolfi, L., Ellero, A., Ottria, G., Catanzariti, R., Tekin, U.K., Sayit, K., 2014. The Arkot Dağ Mélange in Araç area, central Turkey: evidence of its origin within the geodynamics evolution of the Intra-Pontide Suture Zone. J. Asian Earth Sci. 85, 117–139.
Gudmundsson, A., Brenner, S.L., 2001. How hydrofractures become arrested. Terra Nova 13 (6), 456–462.
Gudmundsson, A., Fjeldskaar, I., Brenner, S.L., 2002. Propagation pathways and fluid transport of hydrofractures in jointed and layered rocks in geothermal fields. J. Volcanol. Geotherm. Res. 116 (3–4), 257–278.
Güleç, N., Hilton, D.R., Mutlu, H., 2002. Helium isotope variations in Turkey: relationship to tectonics, volcanism and recent seismic activities. Chem. Geol. 187, 129–142.
Hancock, P.L., Charmes, R.M.L., Altunel, E., Çakır, Z., 1999. Travitonics: using travertines in active fault studies. J. Struct. Geol. 21, 903–916.
Hartleb, R.D., Dolan, J.F., Kozacı, O., Akyüz, H.S., Seitz, G.G., 2006. A 2500-yr-long

paleoseismologic record of large, infrequent earthquakes on the North Anatolian fault at Cukurcimen, Turkey. Bull. Seismol. Soc. Am. 118, 823–840.
Heidbach, O., Custodio, S., Kingdon, A., Mariucci, M.T., Montone, P., Müller, B., Pierdominici, S., Rajabi, M., Reinecker, J., Reiter, K., Tingay, M., Williams, J., Ziegler, M., 2016. Stress Map of the Mediterranean and Central Europe 2016. GFZ Data Services.
Herbert, J.W., Cooke, M.L., Oskin, M., Difo, O., 2014. How much can off-fault deformation contribute to the slip rate discrepancy within the eastern California shear zone? Geology 42 (1), 71–74.
Hilton, D.R., Fischer, T.P., Marty, B., 2002. Noble gases and volatile recycling at subduction zones. In: In: Porcelli, D., Ballentine, C.J., Wieler, R. (Eds.), Noble Gases and Volatile Recycling at Subduction Zones, vol. 47. Mineralogical Society of America, Washington, DC, Reviews in Mineralogy and Geochemistry, pp. 319–370.
Huang, W.L., Longo, J.M., 1994. Experimental studies of silicate–carbonate reactions. 2. Applications to steam flooding of oil sands. Appl. Geochem. 9 (5), 523–532.
Inguaggiato, S., Rizzo, A., 2004. Dissolved helium isotope ratios in ground-waters: a new technique based on gas-water re-equilibration and its application to a volcanic area. Appl. Geochem. 19, 665–673.
Jones, B., 2017a. Review of aragonite and calcite crystal morphogenesis in thermal spring systems. Sed. Geol. 354, 9–23.
Jones, B., 2017b. Review of calcium carbonate polymorph precipitation in spring systems. Sed. Geol. 353, 64–75.
Jones, B., Peng, 2016. Mineralogical, crystallographic, and isotopic constraints on the precipitation of aragonite and calcite at Shiqiang and other hot springs in Yunnan Province, China. Sediment. Geol. 345, 103–125.
Kaduri, M., Gratier, J.-P., Lesser, C., Çakır, Z., Renard, F., 2019. Quantifying the partition between seismic and aseismic deformation along creeping and locked sections of the North Anatolian fault, Turkey. Pure Appl. Geophys. https://doi.org/10.1007/s00024-018-2027-2.
Karabacak, V., Altunel, E., Çakır, Z., 2011. Monitoring aseismic surface creep along the North Anatolian Fault (Turkey) using ground-based LIDAR. Earth Planet. Sci. Lett. 304, 64–70.
Karabacak, V., Uysal, I.T., Ünal-İmer, E., Mutlu, H., Zhao, J., 2017. U-Th age evidence from carbonate veins for episodic crustal deformation of Central Anatolian Volcanic Province. Quat. Sci. Rev. 177, 158–172.
Karabacak, V., Uysal, I.T., Mutlu, H., Ünal-İmer, E., Dirik, R.K., Feng, Y.-X., Akıska, S., Aydoğdu, İ., Zhao, J.-X., 2019. Are U-Th dates correlated with historical records of earthquakes? Constraints from co-seismic carbonate veins within the North Anatolian Fault Zone. Tectonics 38 (7), 2431–2448.
Kele, S., Özkul, M., Gökgöz, A., Fórizs, I., Baykara, M.O., Alçiçek, M.C., Németh, T., 2011. Stable isotope geochemical and facies study of Pamukkale travertines: new evidences of low temperature non-equilibrium calcite–water fractionation. Sed. Geol. 238, 191–212.
Kele, S., Breitenbach, S.F.M., Capezzuoli, E., Meckler, A.N., Ziegler, M., Millan, I.M., Kluge, T., Deák, J., Hanselmann, K., John, C.M., Yan, H., Liu, Z., Bernasconi, S.M., 2015. Temperature dependence of oxygen and clumped isotope fractionation in carbonates: a study of travertines and tufas in the 6–95 °C temperature range. Geochim. Cosmochim. Acta 168, 172–192.
Kluge, T., John, C.M., Boch, R., Kele, S., 2018. Assessment of factors controlling clumped isotopes and d18O values of hydrothermal vent calcites. Geochem. Geophys. Geosystems 19, 1844–1858.
Kondo, H., Özaksoy, V., Yıldirim, C., 2010. Slip history of the 1944 Bolu-Gerede earthquake rupture along the North Anatolian fault system: implications for recurrence behavior of multisegment earthquakes. J. Geophys. Res. 115, B04316.
Kuterdem, N.K., 2005. Eskipazar (Karabük güneyi) ve Kuzey Anadolu Fay Zonu (KAFZ) arasındaki bölgenin morfo-tektonik özelliklerinin coğrafi bilgi sistemleri ile belirlenmesi. MSc. Thesis. Hacettepe University 94 p, Ankara (in Turkish).
Lawrence, M.G., Kamber, B.S., 2006. The behaviour of the rare earth elements during estuarine mixing-revisited. Mar. Chem. 100, 147–161.
Ludwig, K.R., 2003. Users Manual for Isoplot/Ex Version 3.0: A Geochronological Toolkit for Microsoft Excel. Berkeley Geochronology Centre, Berkeley (Special Publication No. 3).
McClymont, A.F., Villamor, P., Green, A.G., 2009. Assessing the contribution of off-fault deformation to slip-rate estimates within the Taupo Rift, New Zealand, using 3-D ground-penetrating radar surveying and trenching. Terra Nova 21 (6), 446–451. https://doi.org/10.1111/j.1365-3121.2009.00901.x.
McKenzie, D., 1972. Active tectonics of the Mediterranean Region. Geophys. J. R. Astron. Soc. 30, 109–185.
Mesci, B.L., Gürsoy, H., Tatar, O., 2008. The evolution of travertine masses in the Sivas area (central Turkey) and their relationships to active tectonics. Turk. J. Earth Sci. 17 (2), 19–240.
Möller, P., Dulski, P., Morteani, G., 2003. Partitioning of rare earth elements, yttrium, and some major elements among source rocks, liquid and steam of Larderello –Travale Geothermal Field, Tuscany (Central Italy). Geochim. Cosmochim. Acta 67, 171–183.
Montgomery, D.R., Manga, M., 2003. Stream flow and water well responses to earthquakes. Science 300 (5628), 2047–2049.
Mutlu, H., Güleç, N., 1998. Hydrogeochemical outline of thermal waters and geothermometry applications in Anatolia, Turkey. J. Volcanol. Geotherm. Res. 85, 495–515.
Nuriel, P., Rosenbaum, G., Uysal, I.T., Zhao, J., Golding, S.D., Weinberger, R., Karabacak, V., Avni, Y., 2011. Formation of fault-related calcite precipitates and their implications for dating fault activity in the East Anatolian and Dead Sea Fault Zones. Geol. Soc. London Spec. Publ. 359, 229–248.
Özkul, M., Kele, S., Gökgöz, A., Shen, C., Jones, B., Baykara, M.O., Forizs, I., Nemeth, T., Chang, Y., Alçiçek, M.C., 2013. Comparison of the Quaternary travertine sites in the Denizli extensional basin on their depositional and geochemical data. Sed. Geol. 294, 179–204.
Parkhurst, D.L., Appelo, C.A.J., 2013. Description of Input and Examples for PHREEQC Version 3 – A Computer Program for Speciation, Batch-Reaction, One-Dimensional Transport, and Inverse Geochemical Calculations. U.S. Geol. Surv. Tech. Methods, B. 6, chapter A43, 497 p.. .
Pearce, J.M., et al., 2006. What can we learn from natural analogues? An overview of how analogues can benefit the geological storage of CO_2. In: Lombardi, S. (Ed.), Advances in the Geological Storage of Carbon Dioxide. Springer, Netherlands, pp. 129–139.
Pentecost, A., 2005. Travertine. Springer Verlag, Berlin Heidelberg 446 p.
Ramsay, J.G., 1980. Shear zone geometry: a review. J. Struct. Geol. 2, 83–99.
Ramsay, J.G., Graham, R.H., 1970. Strain variations in shear bands. Can. J. Earth Sci. 7, 786–813.
Rankama, K., Sahama, Th.G., 1950. Geochemistry. University of Chicago Press, Chicago 912 p.
Ren, T., Zhang, X., Han, R., Hou, B., 2015. Carbon–oxygen isotopic covariations of calcite from Langdu skarn copper deposit, China: implications for sulfide precipitation. Chin. J. Geochem. 34 (1), 21–27.
Rimstidt, J.D., Balog, A., Webb, J., 1998. Distribution of trace elements between carbonate minerals and aqueous solutions. Geochim. Cosmochim. Acta 62, 1851–1863.
Robert, F., Boullier, A.M., Firdaous, K., 1995. Gold-quartz veins in metamorphic terranes and their bearing on the role of fluids in faulting. J. Geophys. Res. Solid Earth 100 (B7), 12861–12879.
Rodríguez-Berriguete, A., Alonso-Zarza, A.M., 2019. Controlling factors and implications for travertine and tufa deposition in a volcanic setting. Sed. Geol. 381, 13–28.
Rodríguez-Berriguete, A., Alonso-Zarza, A.M., Cabrera, M.C., Rodríguez-González, A., 2012. The Azuaje travertine: an example of aragonite deposition in a recent volcanic setting, N Gran Canaria Island, Spain. Sed. Geol. 277–278, 61–71.
Rollinson, H.R., 1993. Using Geochemical Data: Evaluation, Presentation, Interpretation, 1st edition. Routledge, London (Longman Scientific and Technical) 352 pp.
Şaroğlu, F., Emre, O., Kuscu, I., 1992. Active Fault Map of Turkey. General Directorate of Mineral Research and Exploration, Ankara.
Şaroğlu, F., Herece, E., Emre, Ö., Sarıaslan, M., 1995. Yeniçağa-Gerede-Eskipazar arasının jeolojisi ve Kuzey Anadolu Fayı'nın genel özellikleri, Maden Tetkik ve Arama Genel Müdürlüğü (MTA). Report No. 9873 (unpublished, in Turkish). .
Şengör, A.M.C., Yilmaz, Y., 1981. Tethyan evolution of Turkey – a plate tectonic approach. Tectonophysics 75 (3–4), 181–241.
Şengör, A.M.C., Zabcı, C., 2019. In: Kuzucuoğlu, C., Çiner, A., Kazancı, N. (Eds.), The North Anatolian Fault and the North Anatolian Shear Zone, Landscapes and Landforms of Turkey. Springer, pp. 481–494.
Sibson, R.H., 1987. Earthquake rupturing as a mineralizing agent in hydrothermal systems. Geology 15 (8), 701–704.
Sibson, R.H., Moore, J.Mc M., Rankin, A.H., 1975. Seismic pumping a-hydrothermalfluid transport mechanism. J. Geol. Soc. Lond. 131, 653–659.
Süer, S., Güleç, N., Mutlu, H., Hilton, D.R., Çifter, C., Sayin, M., 2008. Geochemical monitoring of geothermal waters (2002–2004) along the North Anatolian Fault Zone, Turkey: spatial and temporal variations and relationship to seismic activity. Pure Appl. Geophys. 165, 17–43.
Tanaka, K., Kawabe, I., 2006. REE abundance in ancient seawater inferred from marine limestone and experimental REE partition coefficients between calcite and aqueous solution. Geochem. J. 40, 425–435.
Taylor, R.S., McLennan, S.M., 1985. The Continental Crust: Its Composition and Evolution. Blackwell, Oxford, pp. 312.
Titus, S.J., Dyson, M., DeMets, C., Tikoff, B., Rolandone, F., Bürgmann, R., 2011. Geologic versus geodetic deformation adjacent to the San Andreas fault, central California. Geol. Soc. Am. Bull. 123 (5–6), 794–820. https://doi.org/10.1130/b30150.1.
Tokay, M., 1973. Kuzey Anadolu Fay Zonunun Gerede ile Ilgaz arasındaki kısmında jeolojik gözlemler, Kuzey Anadolu Fayı ve Depremler Kuşağı Sempozyumu Tebliğleri. M.T.A. Enstitüsü Ankara, pp. 12–29 (in Turkish).
Ünal–İmer, E., Uysal, I.T., Zhao, J.-X., Işık, V., Shulmeister, J., İmer, A., Feng, Y.-X., 2016. CO2 outburst events in relation to seismicity: constraints from microscale geochronology, geochemistry of late Quaternary vein carbonates, SW Turkey. Geochim. Cosmochim. Acta 187, 21–40.
Uysal, I.T., Feng, Y., Zhao, J.X., Altunel, E., Weatherley, D., Karabacak, V., Cengiz, O., Golding, S.D., Lawrence, M.G., Collerson, K.D., 2007. U-series dating and geochemical tracing of late Quaternary travertine in co-seismic fissures. Earth Planet Sci. Lett. 257, 450–462.
Uysal, I.T., Feng, Y., Zhao, J., Işık, V., Nuriel, P., Golding, S.D., 2009. Hydrothermal CO2 degassing in seismically active zones during the late Quaternary. Chem. Geol. 265, 442–454.
Uysal, I.T., Feng, Y.-X., Zhao, J.-X., Bolhar, R., Isik, V., Baublys, K.A., Yago, A., Golding, S.D., 2011. Seismic cycles recorded in late Quaternary calcite veins: geochronological, geochemical and microstructural evidence. Earth Planet. Sci. Lett. 303, 84–96.
Veizer, J., Compston, W., 1974. $^{87}Sr/^{86}Sr$ composition of seawater during the Phanerozoic. Geochim. Cosmochim. Acta 38, 1461–1484.
Wang, C.-Y., Wang, C.H., Kuo, C.-H., 2004. Temporal change in groundwater level following the 1999 (Mw = 7.5) Chi-Chi earthquake, Taiwan. Geofluids 4 (3), 210–222.
Williams, R.T., Goodwina, L.B., Sharpb, W.D., Mozley, P.S., 2017. Reading a 400,000-year record of earthquake frequency for an intraplate fault. Proc. Natl. Acad. Sci. 114 (19), 4893–4898.
Wilson, M., Tankut, A., Güleç, N., 1997. Tertiary volcanism of the Galatean province, NW Central Anatolia, Turkey. Lithos 42, 105–121.
Yücel, B., Hakyemez, Ş., 1991. Akkaya-Eskipazar (Çankırı) bölgesinin jeolojisi ve jeotermal enerji olanakları:Maden Tetkik ve Arama Genel Müdürlüğü (MTA). Report No. 9427 (unpublished, in Turkish). .
Zhao, J.X., Hu, K., Collerson, K.D., Xu, H.K., 2001. Thermal ionization mass spectrometry U-series dating of a hominid site near Nanjing, China. Geology 29 (1), 27–30.
Zheng, Y.-F., 1990. Carbon-oxygen isotopic covariation in hydrothermal calcite during degassing of CO2. Miner. Depos. 25, 246–250.